Auditory cortex interneuron development requires cadherins operating hair-cell mechanoelectrical transduction.

Baptiste Libé-Philippot, Michel Vittot, Jacques Boutet de Monvel, Sébastien Le Gal, Typhaine Dupont, Paul Avan, Christine Métin, Nicolas Michalski, Christine Petit

Classification : Biological sciences/ Neuroscience

Auditory cortex interneuron development requires cadherins operating hair-cell mechanoelectrical transduction

Short title: Developing auditory cortex and tip-link cadherins

Baptiste Libé-Philippot[1,2,3], Vincent Michel[1,2,3], Jacques Boutet de Monvel[1,2,3], Sébastien Le Gal[1,2,3], Typhaine Dupont[1,2,3], Paul Avan[4,5,6], Christine Métin[7,8,9,*], Nicolas Michalski[1,2,3,*] and Christine Petit[1,2,3,10,11,*,#].

[1]Unité de Génétique et Physiologie de l'Audition, Institut Pasteur, 75015 Paris, France

[2]UMRS 1120, Institut National de la Santé et de la Recherche Médicale (INSERM), 75015 Paris, France

[3]Sorbonne Universités, UPMC Université Paris 06, Complexité du Vivant, 75005 Paris, France

[4]Laboratoire de Biophysique Sensorielle, Université d'Auvergne, 63000 Clermont-Ferrand, France

[5]UMR 1107, Institut National de la Santé et de la Recherche Médicale (INSERM), 63000 Clermont-Ferrand, France

[6]Centre Jean Perrin, 63000 Clermont-Ferrand, France

[7]Institut du Fer à Moulin, 75005 Paris, France

[8]UMRS 839, Institut National de la Santé et de la Recherche Médicale (INSERM), 75005 Paris, France

[9]Sorbonne Universités, UPMC Université Paris 06, Cerveau-Cognition-Comportement (ED3C), 75005 Paris, France

[10]Syndrome de Usher et Autres Atteintes Rétino-Cochléaires, Institut de la Vision, 75012 Paris, France

[11]Collège de France, 75005 Paris, France

* Joint senior authors

#Correspondence: christine.petit@pasteur.fr

Keywords: cadherins, tip links, ankle links, parvalbumin interneurons, audiogenic seizures, neuronal migration, medial ganglionic eminence, auditory cortex, cell polarity, adhesion code, deafness

Abstract

Many genetic forms of congenital deafness affect the sound reception antenna of cochlear sensory cells, the hair bundle. The resulting sensory deprivation jeopardizes auditory cortex (AC) maturation. Early prosthetic intervention should revive this process. Nevertheless, this view assumes that no intrinsic AC deficits coexist with the cochlear ones, a possibility as yet unexplored. We show here that many γ-aminobutyric acid (GABA)ergic interneuron precursors, from their generation in the medial ganglionic eminence up to their settlement in the AC, express two cadherin-related (cdhr) proteins, cdhr23 and cdhr15, that form the hair bundle tip-links gating the mechanoelectrical transduction channels. Mutant mice lacking either protein showed a major decrease in the number of parvalbumin interneurons specifically in the AC, and displayed audiogenic reflex seizures. *Cdhr15*- and *Cdhr23*-expressing interneuron precursors in *Cdhr23*$^{-/-}$ and *Cdhr15*$^{-/-}$ mouse embryos, respectively, failed to enter the embryonic cortex and were scattered throughout the subpallium, consistent with the cell polarity abnormalities we observed *in vitro*. In the absence of adhesion G protein-coupled receptor V1 (adgrv1), another hair bundle link protein, the entry of *Cdhr23*- and *Cdhr15*-expressing interneuron precursors into the embryonic cortex was also impaired. Our results demonstrate that a population of newborn interneurons is endowed with specific cdhr proteins, necessary for these cells to reach the developing AC. We suggest that an “early adhesion code” targets populations of interneuron precursors to restricted neocortical regions belonging to the same functional area. These findings open up new perspectives for auditory rehabilitation and cortical therapies in the patients.

Significance statement

In early-onset genetic forms of deafness, deficits of the auditory sensory organ are sufficient to account for the hearing impairment. However, the possibility that intrinsic deficits of the auditory cortex coexist with the peripheral deficits is still unexplored. We show, in rodents and primates, that the cadherin-related proteins cdhr23 and cdhr15 are expressed by many interneuron precursors targeted specifically to the auditory cortex. A deficiency of either protein results in the failure of these interneuron precursors to enter the embryonic cortex and in abnormally small numbers of parvalbumin interneurons in the auditory cortex only. These findings should lead to an improvement of hearing rehabilitation strategies in patients and open up new genetic approaches for studying auditory cortex development and function.

\body

Introduction

The study of inherited forms of deafness in humans has greatly advanced our understanding of the molecular and cellular mechanisms underlying sound processing in the auditory sensory organ, the cochlea (1). Most mouse models for these deafness forms faithfully reproduce the hearing deficits observed in humans. Furthermore, most of the genetic forms of profound congenital deafness studied to date can be accounted for by deficits of the cochlea. Many of these deafness forms result from structural and functional abnormalities of the hair bundle (2), a tuft of microvillus-like apical protrusions, the stereocilia, forming the mechanosensitive antenna of the sensory hair cells (Fig. S1B).

Early auditory deprivation, such as that due to congenital profound deafness, has major consequences for the maturation of the central auditory system, including the auditory cortex (AC). AC maturation involves successive sensitive periods of cortical plasticity, in which several features, such as the tonotopic organization (sound frequency map) of the AC (3) and the balance between neuronal excitation and inhibition (4), are established under the influence of the acoustic environment (5, 6). This neural plasticity is particularly prominent early in life, shortly after hearing onset, and is jeopardized by the lack of auditory stimulation experienced by children with profound congenital deafness. However, early prosthetic interventions, in which profoundly deaf children are fitted with cochlear implants, restore AC maturation through electrical stimulation of the auditory nerve, as indicated by studies in deaf kittens (7, 8).

Much attention has been focused on the impact of auditory deprivation on AC maturation. However, the possibility that AC intrinsic deficits coexist with peripheral auditory deficits in some genetic forms of deafness has not yet been explored despite the expected impact on rehabilitation in the patients. Such associated central intrinsic deficits would probably be masked by the peripheral deficits. Given the major role played by adhesion proteins in brain development, we addressed this

issue by studying mouse models for two genetic forms of profound congenital deafness resulting from mutations of *CDHR23* and *CDHR15*, encoding two cadherin-related (cdhr) transmembrane proteins, cdhr23 and cdhr15 (also known as cadherin-23 and protocadherin-15, respectively; Fig. S1A-B). Within the hair bundle, cdhr23 and cdhr15, which have unusually long ectodomains (9, 10) (Fig. S1A), interact through their two most amino-terminal cadherin repeats to form an overlapped, antiparallel heterodimer (11). They form the tip links (12), fine filaments connecting the tip of a stereocilium to the side of the adjacent taller stereocilium that convey sound-evoked mechanical forces to the mechanoelectrical transduction channels. They also form transient lateral links connecting the stereocilia together, and some of the stereocilia with the kinocilium, during hair bundle morphogenesis (13-15) (Fig. S1B). The absence of mechanoelectrical transduction currents in the cochlear hair cells is sufficient to account for the profound deafness of patients lacking either cdhr23 or cdhr15 (12, 16). Our explorations of the expression of cdhr23 and cdhr15 during brain development and of mouse mutants lacking either cdhr protein revealed that both proteins were required for the development of GABAergic interneurons in the AC. The development of these interneurons also required adgrv1 (also known as gpr98, vlgr1, or mass1), which forms another type of hair bundle links, the ankle links.

Results

Cdhr23 and *Cdhr15* are expressed in the MGE-derived interneurons of the developing auditory cortex

We first studied the expression profiles of cdhr23 and cdhr15 in the mouse embryonic telencephalon at the end of corticogenesis, on embryonic day 18.5 (E18.5). Both proteins were detected in the neocortex. Remarkably, immunostaining was restricted to the developing AC (Fig. 1A). The mammalian neocortex contains glutamatergic excitatory neurons (85% of all neocortical neurons in rodents) and γ-aminobutyric acid (GABA)ergic inhibitory interneurons (17, 18). In E18.5 *Nkx2.1*-cre*:Rosa*-tdTomato mice, immunostaining for cdhr23 and cdhr15 in the AC was limited to tdTomato-labeled (tdTomato+) neurons, the GABAergic interneuron precursors that are derived from the *Nkx2.1*-expressing progenitors of the medial ganglionic eminence (MGE) and the preoptic area of the subpallium, the ventral part of the telencephalon (19) (Fig. 1B). About a third of AC tdTomato+ neurons were labeled by anti-cdhr23 or anti-cdhr15 antibodies (30 ± 3%; n = 10 embryos). Almost all these neurons (96 ± 1%; n = 5 embryos on E18.5) stained for one cdhr protein were also stained for the other (Fig. 1C). Immunostaining for cdhr23 and cdhr15 persisted in tdTomato+ interneurons on P5 (Fig. 1D), but had disappeared by P7 (Fig. S2A).

We then examined the expression of *Cdhr23* and *Cdhr15* at earlier stages. Unlike glutamatergic neurons, which are generated in the proliferative ventricular zone of the neocortex and migrate radially to form the future six layers of the cortical plate, neocortical GABAergic interneurons undergo a long migration from their place of birth. They first migrate tangentially within the subpallium, then within the neocortex to reach their final destination, and finally migrate radially to their ultimate cortical layer position (Figs. 1B, 2A) (20, 21). Cdhr23 and cdhr15 were first detected in the telencephalon on E13.5, in newborn tdTomato+ interneuron precursors derived from the ventral MGE mantle zone (Figs. 2A-C, S2B-C), but not in their MKI67-immunoreactive proliferating

progenitors (Fig. 2D) or in the caudal ganglionic eminence (Fig. S2D). Notably, almost all the neurons of the ventral MGE mantle zone stained for one cdhr protein were also stained for the other (Fig. 2E).

Mutant mice deficient for cdhr23 or cdhr15 have abnormally small numbers of parvalbumin interneurons in the auditory cortex

We then investigated whether interneurons expressing parvalbumin (PV) or somatostatin (SST) (22), the two GABAergic interneuron populations derived from *Nkx2.1*-expressing progenitors (23, 24), were affected by the absence of cdhr23 or cdhr15. Markedly fewer PV interneurons were detected in the AC of three-week-old *Cdhr23*$^{-/-}$ mice (2-fold fewer; $P = 0.008$) and *Cdhr15*$^{av\text{-}3J/av\text{-}3J}$ mice (4.2-fold fewer; $P = 0.004$) lacking cdhr23 and cdhr15, respectively, than in the AC of their wild-type littermates (Fig. 3A). By contrast, the numbers of AC SST interneurons were unchanged ($P = 0.14$ and $P = 0.15$ in *Cdhr23*$^{-/-}$ and *Cdhr15*$^{av\text{-}3J/av\text{-}3J}$ mice, respectively; Fig. 3C). Despite the strong reduction in the number of PV interneurons in the AC, the cortical thickness of the AC in wild-type (1007 ± 31 µm, n = 8 mice), *Cdhr23*$^{-/-}$ (955 ± 32 µm, n = 8 mice) and *Cdhr15*$^{av\text{-}3J/av\text{-}3J}$ (980 ± 21 µm, n = 8 mice) mice, and the estimated surface of the AC per section in wild-type (1.11 ± 0.09 mm² per section, n = 5 mice), *Cdhr23*$^{-/-}$ (1.16 ± 0.08 mm² per section, n = 5 mice) and *Cdhr15*$^{av\text{-}3J/av\text{-}3J}$ (1.15 ± 0.06 mm² per section, n = 5 mice) mice, were similar ($P > 0.4$ for all comparisons).

We asked whether this major PV interneuron deficit resulted from the absence of cochlear mechanoelectrical transduction in *Cdhr23*$^{-/-}$ and *Cdhr15*$^{av\text{-}3J/av\text{-}3J}$ mice, by studying *Cdhr23*$^{+/-}$ and *Cdhr15*$^{+/av\text{-}3J}$ heterozygous mice, which have no cochlear deficit (25) (Fig. S3A-B). At three to four weeks of age, these mice also had fewer PV interneurons in the AC, with interindividual variation, than wild-type mice (1.6-fold and 1.8-fold fewer, on average, respectively; $P < 10^{-3}$; Fig. 3B). PV interneuron deficits are often implicated in seizure disorders (26). We therefore investigated the susceptibility of *Cdhr23*$^{+/-}$ and *Cdhr15*$^{+/av\text{-}3J}$ mice to audiogenic seizures, reflex seizures triggered by

loud sounds (27). Audiogenic seizures were observed in a large proportion of *Cdhr23*$^{+/-}$ (51%, n = 49) and *Cdhr15*$^{+/av\text{-}3J}$ (38%, n = 50) mice, but not in their wild-type littermates (n = 40 and n = 36, respectively; $P < 10^{-4}$ for both comparisons). These seizures occurred only in mice with at least a 1.6-fold decrease in the number of PV interneurons in the AC ($P < 10^{-4}$ for both comparisons; Fig. 3B). This susceptibility was not linked to the sex of the affected mice (10 of 20 females and 11 of 23 males for affected *Cdhr23*$^{+/-}$ mice, P = 0.87; 6 of 20 females and 13 of 24 males for affected *Cdhr15*$^{+/av\text{-}3J}$ mice, P = 0.19) or that of the parent transmitting the mutation (14 of 25 and 10 of 18 offspring produced by *Cdhr23*$^{+/-}$ mothers and fathers, respectively, P = 0.77; 6 of 15 and 13 of 29 offspring produced by *Cdhr15*$^{+/av\text{-}3J}$ mothers and fathers, respectively , P = 0.98). In contrast, the numbers of SST interneurons were normal in the AC of *Cdhr23*$^{+/-}$ and *Cdhr15*$^{+/av\text{-}3J}$ mice (P = 0.91 and P = 0.85, respectively; Fig. 3C). Notably, the numbers of PV interneurons in the somatosensory and motor cortices were unaffected in *Cdhr23*$^{+/-}$ and *Cdhr15*$^{+/av\text{-}3J}$ mice (P = 0.63, P = 1, P = 0.11, P = 0.85 in the somatosensory cortex of *Cdhr23*$^{+/-}$ and *Cdhr15*$^{+/av\text{-}3J}$ mice and in the motor cortex of *Cdhr23*$^{+/-}$ and *Cdhr15*$^{+/av\text{-}3J}$ mice, respectively; Fig. 3D-E). Thus, the absence of cdhr23 or cdhr15 severely impairs the development of PV interneurons in the AC but not in other cortices.

Mutant mice deficient for cdhr23 or cdhr15 in GABAergic interneurons have abnormally small numbers of PV interneurons in the auditory cortex

We looked for the origin of the PV interneuron deficit in *Cdhr23*$^{-/-}$ and *Cdhr15*$^{av\text{-}3J/av\text{-}3J}$ mice. We used *Nkx2.1*-cre:*Rosa*-tdTomato mice (19) to conditionally inactivate *Cdhr23* and *Cdhr15* in MGE-derived interneuron precursors. *Nkx2.1* is transiently expressed by cortical interneuron precursors of the MGE and preoptic area, which give rise to all the PV and SST interneurons of the neocortex (19, 28). We crossed *Nkx2.1*-cre:*Rosa*-tdTomato mice (19) with either *Cdhr23*$^{lox/lox}$ mice (29) or *Cdhr15*$^{lox/lox}$ mice to obtain *Nkx2.1*-cre:*Rosa*-tdTomato; *Cdhr23*$^{lox/lox}$ mutant mice, or *Nkx2.1*-cre:*Rosa*-tdTomato; *Cdhr15*$^{lox/lox}$ mutant mice (hereafter referred to as *Cdhr23* cKO or *Cdhr15* cKO

mice). *Cdhr23*$^{lox/lox}$ or *Cdhr15*$^{lox/lox}$ littermates that do not express *cre*, or *Nkx2.1*-cre:*Rosa*-tdTomato mice, were used as controls. On P27, audiogenic seizures were detected in 87% of *Cdhr23* cKO mice (n = 18) and 73% of *Cdhr15* cKO mice (n = 15), but in none of their control littermates ($P < 10^{-5}$ and $P < 10^{-3}$ for *Cdhr23* cKO and *Cdhr15* cKO mice, respectively). Markedly fewer PV interneurons were detected in the AC of P27 *Cdhr23* cKO (2.3-fold fewer; $P = 0.008$) and *Cdhr15* cKO mice (2.4-fold fewer; $P = 0.008$) than in *Nkx2.1*-cre:*Rosa*-tdTomato mice (Figs. 4A-B, S4). In contrast, the numbers of SST interneurons in the AC were normal in *Cdhr23* cKO ($P = 0.69$) and *Cdhr15* cKO mice ($P = 0.22$; Fig. 4A-B). The numbers of tdTomato+ interneurons, in which PV or SST were not detected, were unchanged in *Cdhr23* cKO ($P = 0.42$) and *Cdhr15* cKO mice ($P = 0.15$; Fig. 4A-B), which excludes the possibility that a mere loss of PV expression without loss of interneurons could account for the abnormally small number of PV interneurons. This demonstrates that the deficit of PV interneurons in the AC results from the lack of expression of *Cdhr23* or *Cdhr15* in MGE-derived interneuron precursors.

Loss of PV interneurons upon *in situ* deletion of *Cdhr15* in the temporal cortex of newborn mice

We then assessed the role of cdhr23 and cdhr15 at early postnatal stages, by studying the impact of a postnatal *in situ* deletion of *Cdhr15* in the temporal cortex. A lentiviral vector encoding a cre recombinase fused to the green fluorescent protein (LV-*cre-GFP*) was injected into the temporal cortex of *Cdhr15*$^{lox/lox}$ mice on P1 (LV-*cre-GFP* P1-injected *Cdhr15*$^{lox/lox}$ mice), when immature neurons begin to form synapses (30). Cdhr15 and cdhr23 were no longer detected in the AC of these mice on P5 (Fig. 5A). Moreover, in these mice, but not in LV-*cre-GFP* P1-injected wild-type mice, many AC neurons stained for both GFP and the GABAergic interneuron marker Dlx5 (31), expressed, mostly in layer IV, caspase-3, a protein involved in cell apoptosis (Fig. S5B). On P24, audiogenic seizures were observed in all LV-*cre-GFP* P1-injected *Cdhr15*$^{lox/lox}$ mice ($n = 12$), but not in LV-*cre-GFP* P1-injected wild-type mice ($n = 7$; $P < 10^{-4}$) or other controls including non-injected

Cdhr15$^{lox/lox}$ mice (n = 8, $P < 10^{-4}$), LV-*GFP* P1-injected *Cdhr15*$^{lox/lox}$ mice (n = 4, $P < 10^{-3}$), and *Cdhr15*$^{lox/lox}$ mice receiving LV-*cre*-*GFP* injection into the temporal cortex on P10 (n = 8, $P < 10^{-4}$) or into the motor cortex on P1 (n = 9, $P < 10^{-4}$). LV-*cre*-*GFP* P1-injected *Cdhr15*$^{lox/lox}$ mice that received injection in the temporal cortex had markedly fewer PV interneurons in the AC (2.6-fold fewer) than LV-*cre*-*GFP* P1-injected wild-type mice (n = 6 for both genotypes; P = 0.004; Fig. 5B-C), with unaffected ABR thresholds (Fig. S5A). Thus, PV interneuron deficits restricted to the AC can cause audiogenic seizures. Moreover, these results demonstrate the crucial role of cdhr15 in the survival of immature interneurons of the AC that give rise to PV interneurons.

A population of interneuron precursors requires both cdhr23 and cdhr15 to enter the embryonic cortex

We then investigated a possible role of cdhr23 and cdhr15 in the early development of cortical interneurons. On E14.5-E15.5, in *Nkx2.1*-cre:*Rosa*-tdTomato embryos, tdTomato+ interneuron precursors expressing *Cdhr23* (cdhr23+) and/or *Cdhr15* (cdhr15+) were detected within the subpallium and along the superficial and deep tangential migratory routes of interneurons in the developing cortex (23) (Figs. 6A, S1C, S7A). In contrast to the postnatal *in situ* deletion of *Cdhr15* that led to the lack of expression of *Cdhr23* in the developing AC, interneuron precursors of *Cdhr23*$^{-/-}$ and *Cdhr15*$^{-/-}$ embryos each retained the expression of cdhr15 and cdhr23, respectively. Remarkably, on E14.5, cdhr15+ and cdhr23+ neurons in *Cdhr23*$^{-/-}$ and *Cdhr15*$^{-/-}$ embryos, respectively, were abnormally scattered throughout the subpallium (Fig. 6B), with no signs of apoptosis (Fig. S6A). They were absent from the embryonic cortex, whereas the streams of tangentially migrating neurons stained for doublecortin appeared unaffected (Fig. S6B). The fluorescence ratio between cdhr signals in the embryonic cortex and subpallium was much lower in *Cdhr23*$^{-/-}$ (0.07 ± 0.04, n = 5) and *Cdhr15*$^{-/-}$ (0.17 ± 0.05, n = 5) embryos than in wild-type embryos

(1.2 ± 0.07, n = 7; P = 0.003 for both comparisons). Thus, both cdhr23 and cdhr15 play crucial roles in the migration of MGE-derived interneuron precursors towards the embryonic cortex.

Cell polarity defects in *Cdhr23*$^{-/-}$ and *Cdhr15*$^{-/-}$ MGE-derived interneuron precursors

We therefore explored whether the absence of cdhr23 or cdhr15 affected the migration of MGE-derived interneuron precursors on synthetic substrates *in vitro*. Cdhr15+ or cdhr23+ neurons leaving E13.5 *Cdhr23*$^{-/-}$ or *Cdhr15*$^{-/-}$ MGE explants, respectively, cultured on a laminin substrate, migrated over much smaller areas (2.4-fold and 6.7-fold smaller, respectively) than cdhr23+/cdhr15+ neurons leaving wild-type MGE explants ($P < 10^{-2}$ for both comparisons; Fig. S7B). By contrast, the migration area was unaffected by culturing MGE explants on a cadherin-2 (cdh2, N-cadherin)/laminin substrate stimulating neurite outgrowth *in vitro* (32) (see Methods; $P > 0.4$ for both comparisons; Fig. S7C). Both cdhr23 and cdhr15 were localized at the leading processes and growth cones (Figs. 6C, S7D-E). They were coexpressed in 87% of the neurons leaving E13.5 wild-type MGE explants that express cdhr23 and/or cdhr15 (n = 108 neurons). The percentage of neurons with more than one process was three times greater in cdhr15+ neurons leaving *Cdhr23*$^{-/-}$ explants (18%, n = 131 neurons; P = 0.004) than in cdhr23+/cdhr15+ neurons leaving wild-type explants (6%, n = 113 neurons), but was unaffected in cdhr23+ neurons leaving *Cdhr15*$^{-/-}$ explants (n = 118 neurons; P = 0.74; Fig. 6C). In cdhr23+ neurons migrating from *Cdhr15*$^{-/-}$ explants, however, the centrosome was randomly distributed around the nucleus rather than preferentially facing the leading process as in cdhr23+/cdhr15+ neurons migrating from wild-type explants (Kolmogorov-Smirnov test, $P < 10^{-3}$; Fig. 6C) and cdhr15+ neurons migrating from *Cdhr23*$^{-/-}$ explants (Kolmogorov-Smirnov test, P = 0.95). These cell polarity deficits of newborn interneurons are consistent with the *in vivo* misrouting of interneuron precursors (32) in *Cdhr23*$^{-/-}$ and *Cdhr15*$^{-/-}$ embryos (Fig. 6B). They suggest that both cdhr23 and cdhr15 contribute to interneuron precursor cell polarity, but through different activities.

Impaired entry of MGE-derived GABAergic interneurons expressing cdhr23 and cdhr15 into the embryonic cortex of mutant mice lacking adgrv1

We then asked whether the hair bundle of auditory hair cells and the interneurons of the auditory cortex share other critical proteins for their respective development. Based on the susceptibility to audiogenic seizures of *Adgrv1*$^{-/-}$ mice, which have a moderate hearing impairment on P20-P30 (33-35), we focused on adgrv1, a member of the adhesion G-protein-coupled receptor family with a very long extracellular region that forms transient lateral links between stereocilia, the ankle links, during hair bundle development (36, 37) (Fig. S1A-B). On P24, audiogenic seizures were observed in all *Adgrv1*$^{-/-}$ mice (n = 36), but none of the *Adgrv1*$^{+/-}$ mice (n = 21; $P < 10^{-13}$). *Adgrv1*$^{-/-}$ mice also had fewer PV interneurons in the AC than their *Adgrv1*$^{+/-}$ littermates (3.1-fold fewer, n = 5 for both genotypes, P = 0.008; Fig. 7A), but normal numbers of AC SST interneurons (P = 0.2; Fig. 7B).

In E13.5-E14.5 mice, adgrv1 was detected in the subpallium, including the mantle zone of the MGE and the MGE ventricular zone containing MKI67-labeled progenitors (Figs. 7C, S8A). On E18.5, adgrv1 was mostly detected in the nestin-labeled processes of radial glial cells in the AC (Fig. S8B). In E14.5 *Adgrv1*$^{-/-}$ mice, the entry of neurons expressing cdhr23 and cdhr15 into the embryonic cortex was impaired (Fig. 7D). The fluorescence ratio between cdhr-immunoreactive signals in the embryonic cortex and subpallium was 34% lower in *Adgrv1*$^{-/-}$ embryos (0.8 ± 0.04, n = 7) than in wild-type embryos (1.2 ± 0.07, n = 7, $P < 10^{-3}$). Thus, adgrv1 is also involved in the development of PV interneurons in the AC, and in the entry of cdhr23- and cdhr15-expressing interneuron precursors into the embryonic cortex.

Similar expression profiles of cdhr23, cdhr15, and adgrv1 in mouse and macaque

Finally, we addressed the issue of the conservation of expression profiles for cdhr23, cdhr15, and adgrv1 in primate embryos. In E63 macaque embryos (equivalent to E13-E14 mice (38)), the

three proteins were immunodetected in the MGE (Fig. 8A). On E85 (equivalent to E17-E18 in the mouse) (38), cdhr23 and cdhr15 were detected in Dlx5-immunoreactive GABAergic interneuron precursors of the AC (31) (Figs. 8B-C, S9), and adgrv1 was detected in the nestin-labeled processes of AC radial glial cells (Figs. 8B, 8D, S9). The expression profiles of cdhr23, cdhr15, and adgrv1 in the embryonic telencephalon are thus similar in mouse and macaque.

Discussion

Our results reveal that AC interneuron development is impaired in mutant mice defective for *Cdhr23, Cdhr15,* or *Adgrv1*. The lack of cdhr23, cdhr15, or adgrv1 in these mice affects the entry of *Cdhr15*-, *Cdhr23*- and *Cdhr23*-/*Cdhr15*-expressing interneuron precursors, respectively, into the embryonic cortex, leading to a greatly decreased number of PV interneurons in the AC (Fig. S1).

The observed interneuron precursor migration deficits are not a consequence of the peripheral auditory impairment present in *Cdhr23*$^{-/-}$, *Cdhr15*$^{av\text{-}3J/av\text{-}3J}$, and *Adgvr1*$^{-/-}$ mice (12-14), because they are detectable as early as E.14.5, long before the onset of hearing (~P12-P13 in mice). The abnormally small number of PV interneurons in the AC and the susceptibility to audiogenic seizures induced by the *in situ* deletion of *Cdhr15* in the temporal cortex on P1 revealed an additional intrinsic role of cdhr15 in the developing AC before the onset of hearing. Given the co-expression of *Cdhr23* and *Cdhr15* in immature interneurons of the AC, and the lack of expression of *Cdhr23* on P5 after the deletion of *Cdhr15*, cdhr23 probably plays a similar role in the early postnatal AC. Finally, a cortical origin for the PV interneuron deficit in the AC is further supported by the observation of a similar defect in *Cdhr23*$^{+/-}$ and *Cdhr15*$^{+/av\text{-}3J}$ mice and in *Cdhr23* cKO and *Cdhr15* cKO mice, which have no peripheral hearing deficit.

Converging lines of evidence indicate that the *Cdhr23*- and *Cdhr15*-expressing interneuron precursors of the MGE develop into PV interneurons of the AC. *Cdhr23*- and *Cdhr15*-expressing interneuron precursors are found in the ventral part of the MGE on E13.5, the time and place at which future cortical PV interneurons are generated (39). From E13.5 to P7, labeling for cdhr23 and cdhr15 is limited to MGE-derived interneuron precursors, which mature into PV and SST interneurons. By P5, *Cdhr23*- and *Cdhr15*-expressing interneuron precursors are mostly found accumulated in cortical layer IV in the AC, the preferential location of PV interneurons (40). The number of SST interneurons, the other subclass of MGE-derived interneurons, was not affected in *Cdhr23, Cdhr15,* and *Adgrv1* mutant mice. Moreover, *Cdhr23* and *Cdhr15* expression in interneuron

precursors was found to be restricted to the developing AC on E18.5, like the decrease in the number of PV interneurons in three-week-old *Cdhr23* and *Cdhr15* mutant mice. Finally, the conditional deletion of *Cdhr23* and *Cdhr15* in MGE-derived interneurons at the progenitor stage reproduced the PV interneuron deficit and led to a susceptibility to audiogenic seizures. Together, these results demonstrate that the population of *Cdhr23*- and *Cdhr15*-expressing interneuron precursors of the MGE gives rise to a large fraction of the PV interneurons in the AC.

The numbers of PV interneurons in the AC of $Cdhr23^{+/-}$ and $Cdhr15^{+/av\text{-}3J}$ mice, although systematically small, differed strongly between individual mice, as did susceptibility to audiogenic seizures. The origin of this heterogeneity remains unclear, but was not related to the sex of the affected heterozygous mouse or of the parent transmitting the mutation (which would have suggested genomic imprinting of *Cdhr23* and *Cdhr15*). Genetic background or a random monoallelic expression of *Cdhr23* and *Cdhr15* in the telencephalon (already reported for both genes in neural progenitor cells derived from mouse embryonic stem cells (41)), may account for this variability.

What roles do cdhr23 and cdhr15 play in interneuron precursors? Migration areas were markedly smaller for $cdhr15^{+}$ interneuron precursors and $cdhr23^{+}$ interneuron precursors growing out of $Cdhr23^{-/-}$ and $Cdhr15^{-/-}$ MGE explants cultured on laminin substrate, respectively, than for $cdhr23^{+}$/$cdhr15^{+}$ interneuron precursors growing out of wild-type MGE explants, suggesting a motility deficit and/or a polarity defect of these migrating neurons. The migration areas observed on a substrate consisting of cdh2 and laminin, promoting the motility of interneuron precursors, were no smaller than normal, but neurons lacking either cdhr23 or cdhr15 displayed cell polarity defects, albeit with different manifestations. These cell polarity defects are consistent with the dispersion of these interneuron precursors in the subpallium of mutant embryos. On P1, a developmental time-point at which interneuron precursors have reached their final AC destination, the *in situ* deletion of *Cdhr15* in the temporal cortex led to apoptosis of local interneuron precursors. This additional role of cdhr15 may reflect the early involvement of this cdhr in GABAergic interneuron synaptogenesis,

which is considered to be essential for interneuron survival (42). This dual role is reminiscent of that reported for two other adhesion proteins in GABAergic interneuron precursors in the embryonic telencephalon: celsr3 (also known as adgrc3) (43) from the flamingo cadherin (9) and adhesion G-protein coupled receptor families (44), and cdh2 (32). However, these two proteins are not required for the specific targeting of interneuron precursors to a particular neocortical area. Cdh2 is critically involved in the cell polarity and migration of GABAergic interneuron precursors, whereas celsr3 is required for the entry of interneuron precursors expressing calbindin-2 (also known as calretinin) into the embryonic cortex, and both proteins are also involved in synaptogenesis (45, 46).

Previous studies have shown that most clonally related interneurons derived from the MGE are targeted to one telencephalon structure (47-49), where they form clusters (50, 51). Regardless of the possible clonal relationship between *Cdhr23*-/*Cdhr15*-expressing GABAergic interneuron precursors in the AC, our results indicate that these precursors are targeted specifically to the AC immediately after their birth. Based on the critical role of adhesion proteins cdhr23 and cdhr15 in the targeting and survival of newly born GABAergic interneuron precursors in a specific cortical area, the developing AC, reported here for the first time, we suggest that there is an “adhesion code”, which functions early in development and targets particular populations of newborn MGE-derived GABAergic interneuron precursors to functionally specific areas of the neocortex.

The conservation, from mouse to macaque, of the expression profiles of the three proteins studied here suggests the existence of an intrinsic deficit of PV interneurons in the AC of humans carrying *CDHR23*, *CDHR15*, or *ADGRV1* mutations, despite differences in the origin of these neurons in the human brain (52). After the fitting of cochlear implants, some of these patients have been reported to face unusual speech-recognition difficulties not observed in patients with mutations of other deafness genes (53). These difficulties might be related to the involvement of PV interneurons in the experience-driven neural plasticity underlying AC maturation (8, 54) and the temporal precision of sound detection critical for speech perception (55). The shaping of the

perception of several acoustic features throughout life, including frequency discrimination acuity (56) and the detection of unexpected sounds, also involves PV interneurons of the AC (57).

The results presented here suggest the possible involvement of other deafness genes underlying peripheral auditory deficits in the development and functioning of the AC. Mutations of *CDHR23* or *CDHR15*, and of *ADGRV1* are responsible for type 1 and type 2 Usher syndrome, respectively. These autosomal recessive disorders combine congenital hearing impairment with delayed-onset sight loss. The formation of protein complexes containing cdhr23, cdhr15, or adgrv1 together with other Usher syndrome gene products in both hair cells and photoreceptor cells (58-60) identifies these proteins as attractive candidates for involvement in AC interneuron development. Broadening our view by identifying the other proteins involved will help to clarify the evolutionary steps accounting for the use of the same essential proteins for the development of the cochlea and the auditory cortex.

The impact of sensory deprivation on AC development in people with genetic forms of deafness has so far overshadowed the consideration of possible intrinsic cortical deficiencies. Advances in our understanding of the hidden intrinsic cortical deficits of hereditary forms of deafness should provide a scientific basis for improving auditory rehabilitation in patients and for the development of cortical therapies. This work should also pave the way to the development of a genetic approach to the cellular and molecular mechanisms involved in AC development and functioning.

Materials and methods

A detailed description of the methods is available in SI Appendix, Materials and Methods. Animal experiments were carried out in accordance with French and European regulations. Approval for the experiments using animals was obtained from the Animal Use Committee of Institut Pasteur. Susceptibility to audiogenic seizures was evaluated using high-intensity (100-110 dB) continuous pure tones (8-15 kHz) lasting up to one minute. Hearing tests were performed as described in (61, 62). For immunofluorescence analyses, the antibodies directed against cdhr23 and cdhr15 were used as described in (16, 59). Culture of MGE explants and quantification of neuronal migration were carried out as described in (32).

Acknowledgments

We thank M. Bosch Grau, S. Chardenoux, A. Emptoz, C. Leclech, D. Oficjalska, M. Pedraza Boti, E. Pepermans, C. Trébeau, and D. Weil for assistance with this project, and J.-P. Hardelin for his important contribution to the writing of the manuscript. We warmly thank S. Etienne-Manneville (Institut Pasteur, Paris, France) and S. Garel (Ecole Normale Supérieure, Paris, France) for advice. We thank G. Lepousez (Institut Pasteur, Paris, France) and N. Renier (Institut du Cerveau et de la Moelle Epinière, Paris, France) for critical reading of the manuscript. We thank C. Dehay (PrimaLyon Platform, Institut Cellule Souche et Cerveau, INSERM, Bron, France), N. Kessaris (University College London, United Kingdom), and M. Sato (University of Fukui, Japan) for sharing brain sections from macaque embryos, *Nkx2.1*-cre:*Rosa*-tdTomato mice, and *Adgrv1*^{tm1Msat} mice, respectively. We gratefully acknowledge the Imagopole-Citech facility (Institut Pasteur, Paris, France), which is part of the France BioImaging infrastructure supported by the French National Research Agency (ANR-10-INSB-04-01, *Investissements d'Avenir* program), for the use of their microscopes. This work was supported by PhD funding for BLP from the French Ministry of Research, attributed by the Ecole Normale Supérieure (Paris, France), the *Prix Emergence* and the

SEIZEAR grant of the *Agir Pour l'Audition* foundation to NM, and grants from the French Agence Nationale pour la Recherche (ANR) as part of the second *Investissements d'Avenir* program LIGHT4DEAF [ANR-15-RHUS-0001] and the LabEx LIFESENSES [ANR-10-LABX-65], the European Research Council (ERC-2011-ADG_294570) to CP, the BNP Paribas Foundation, the FAUN Stiftung and the LHW-Stiftung.

Author contributions

CP, NM, and CM designed the study; BLP, VM, JBM, PA, SLG and TD performed research; BLP, JBM, CM, NM, and CP analyzed data; CP, NM, CM and BLP wrote the paper.

References

1. Petit C (1996) Genes responsible for human hereditary deafness: symphony of a thousand. *Nat Genet* 14(4):385-391.
2. Richardson GP, de Monvel JB, & Petit C (2011) How the genetics of deafness illuminates auditory physiology. *Annu Rev Physiol* 73:311-334.
3. Zhang LI, Bao S, & Merzenich MM (2001) Persistent and specific influences of early acoustic environments on primary auditory cortex. *Nat Neurosci* 4(11):1123-1130.
4. Dorrn AL, Yuan K, Barker AJ, Schreiner CE, & Froemke RC (2010) Developmental sensory experience balances cortical excitation and inhibition. *Nature* 465(7300):932-936.
5. de Villers-Sidani E & Merzenich MM (2011) Lifelong plasticity in the rat auditory cortex: basic mechanisms and role of sensory experience. *Prog Brain Res* 191:119-131.
6. Sanes DH & Bao S (2009) Tuning up the developing auditory CNS. *Curr Opin Neurobiol* 19(2):188-199.
7. Klinke R, Kral A, Heid S, Tillein J, & Hartmann R (1999) Recruitment of the auditory cortex in congenitally deaf cats by long-term cochlear electrostimulation. *Science* 285(5434):1729-1733.
8. Kral A, Kronenberger WG, Pisoni DB, & O'Donoghue GM (2016) Neurocognitive factors in sensory restoration of early deafness: a connectome model. *Lancet Neurol*.
9. Hulpiau P, Gul IS, & van Roy F (2013) New insights into the evolution of metazoan cadherins and catenins. *Prog Mol Biol Transl Sci* 116:71-94.
10. Hulpiau P & van Roy F (2009) Molecular evolution of the cadherin superfamily. *Int J Biochem Cell Biol* 41(2):349-369.
11. Sotomayor M, Weihofen WA, Gaudet R, & Corey DP (2012) Structure of a force-conveying cadherin bond essential for inner-ear mechanotransduction. *Nature* 492(7427):128-132.
12. Kazmierczak P, *et al.* (2007) Cadherin 23 and protocadherin 15 interact to form tip-link filaments in sensory hair cells. *Nature* 449(7158):87-91.
13. Lefevre G, *et al.* (2008) A core cochlear phenotype in USH1 mouse mutants implicates fibrous links of the hair bundle in its cohesion, orientation and differential growth. *Development* 135(8):1427-1437.
14. Petit C & Richardson GP (2009) Linking genes underlying deafness to hair-bundle development and function. *Nat Neurosci* 12(6):703-710.
15. Goodyear RJ, Forge A, Legan PK, & Richardson GP (2010) Asymmetric distribution of cadherin 23 and protocadherin 15 in the kinocilial links of avian sensory hair cells. *J Comp Neurol* 518(21):4288-4297.
16. Pepermans E, *et al.* (2014) The CD2 isoform of protocadherin-15 is an essential component of the tip-link complex in mature auditory hair cells. *EMBO Mol Med* 6(7):984-992.
17. Defelipe J (2011) The evolution of the brain, the human nature of cortical circuits, and intellectual creativity. *Front Neuroanat* 5:29.
18. Markram H, *et al.* (2004) Interneurons of the neocortical inhibitory system. *Nat Rev Neurosci* 5(10):793-807.
19. Kessaris N, *et al.* (2006) Competing waves of oligodendrocytes in the forebrain and postnatal elimination of an embryonic lineage. *Nat Neurosci* 9(2):173-179.
20. Marin O & Muller U (2014) Lineage origins of GABAergic versus glutamatergic neurons in the neocortex. *Curr Opin Neurobiol* 26:132-141.
21. Faux C, Rakic S, Andrews W, & Britto JM (2012) Neurons on the move: migration and lamination of cortical interneurons. *Neurosignals* 20(3):168-189.
22. Rudy B, Fishell G, Lee S, & Hjerling-Leffler J (2011) Three groups of interneurons account for nearly 100% of neocortical GABAergic neurons. *Dev Neurobiol* 71(1):45-61.

23. Marin O (2013) Cellular and molecular mechanisms controlling the migration of neocortical interneurons. *Eur J Neurosci* 38(1):2019-2029.
24. Xu Q, Cobos I, De La Cruz E, Rubenstein JL, & Anderson SA (2004) Origins of cortical interneuron subtypes. *J Neurosci* 24(11):2612-2622.
25. Zheng QY, *et al.* (2005) Digenic inheritance of deafness caused by mutations in genes encoding cadherin 23 and protocadherin 15 in mice and humans. *Hum Mol Genet* 14(1):103-111.
26. Houser CR (2014) Do structural changes in GABA neurons give rise to the epileptic state? *Adv Exp Med Biol* 813:151-160.
27. Italiano D, *et al.* (2016) Genetics of reflex seizures and epilepsies in humans and animals. *Epilepsy Res* 121:47-54.
28. Nobrega-Pereira S, *et al.* (2008) Postmitotic Nkx2-1 controls the migration of telencephalic interneurons by direct repression of guidance receptors. *Neuron* 59(5):733-745.
29. Etournay R, *et al.* (2010) Cochlear outer hair cells undergo an apical circumference remodeling constrained by the hair bundle shape. *Development* 137(8):1373-1383.
30. Le Magueresse C & Monyer H (2013) GABAergic interneurons shape the functional maturation of the cortex. *Neuron* 77(3):388-405.
31. Eisenstat DD, *et al.* (1999) DLX-1, DLX-2, and DLX-5 expression define distinct stages of basal forebrain differentiation. *J Comp Neurol* 414(2):217-237.
32. Luccardini C, *et al.* (2013) N-cadherin sustains motility and polarity of future cortical interneurons during tangential migration. *J Neurosci* 33(46):18149-18160.
33. Frings H & Frings M (1951) Otitis media and audiogenic seizures in mice. *Science* 113(2946):689-690.
34. Yagi H, *et al.* (2005) Vlgr1 knockout mice show audiogenic seizure susceptibility. *J Neurochem* 92(1):191-202.
35. Skradski SL, *et al.* (2001) A novel gene causing a mendelian audiogenic mouse epilepsy. *Neuron* 31(4):537-544.
36. McGee J, *et al.* (2006) The very large G-protein-coupled receptor VLGR1: a component of the ankle link complex required for the normal development of auditory hair bundles. *J Neurosci* 26(24):6543-6553.
37. Michalski N, *et al.* (2007) Molecular characterization of the ankle-link complex in cochlear hair cells and its role in the hair bundle functioning. *J Neurosci* 27(24):6478-6488.
38. Dehay C & Kennedy H (2007) Cell-cycle control and cortical development. *Nat Rev Neurosci* 8(6):438-450.
39. Sultan KT, Brown KN, & Shi SH (2013) Production and organization of neocortical interneurons. *Front Cell Neurosci* 7:221.
40. Tremblay R, Lee S, & Rudy B (2016) GABAergic Interneurons in the Neocortex: From Cellular Properties to Circuits. *Neuron* 91(2):260-292.
41. Gendrel AV, *et al.* (2014) Developmental dynamics and disease potential of random monoallelic gene expression. *Dev Cell* 28(4):366-380.
42. Bartolini G, Ciceri G, & Marin O (2013) Integration of GABAergic interneurons into cortical cell assemblies: lessons from embryos and adults. *Neuron* 79(5):849-864.
43. Ying G, *et al.* (2009) The protocadherin gene Celsr3 is required for interneuron migration in the mouse forebrain. *Mol Cell Biol* 29(11):3045-3061.
44. Hamann J, *et al.* (2015) International Union of Basic and Clinical Pharmacology. XCIV. Adhesion G protein-coupled receptors. *Pharmacol Rev* 67(2):338-367.
45. Arikkath J & Reichardt LF (2008) Cadherins and catenins at synapses: roles in synaptogenesis and synaptic plasticity. *Trends Neurosci* 31(9):487-494.
46. Thakar S, *et al.* (2017) Evidence for opposing roles of Celsr3 and Vangl2 in glutamatergic synapse formation. *Proc Natl Acad Sci U S A* 114(4):E610-E618.

47. Mayer C, *et al.* (2015) Clonally Related Forebrain Interneurons Disperse Broadly across Both Functional Areas and Structural Boundaries. *Neuron* 87(5):989-998.
48. Harwell CC, *et al.* (2015) Wide Dispersion and Diversity of Clonally Related Inhibitory Interneurons. *Neuron* 87(5):999-1007.
49. Sultan KT, *et al.* (2016) Clonally Related GABAergic Interneurons Do Not Randomly Disperse but Frequently Form Local Clusters in the Forebrain. *Neuron* 92(1):31-44.
50. Brown KN, *et al.* (2011) Clonal production and organization of inhibitory interneurons in the neocortex. *Science* 334(6055):480-486.
51. Ciceri G, *et al.* (2013) Lineage-specific laminar organization of cortical GABAergic interneurons. *Nat Neurosci* 16(9):1199-1210.
52. Geschwind DH & Rakic P (2013) Cortical evolution: judge the brain by its cover. *Neuron* 80(3):633-647.
53. Wu CC, *et al.* (2015) Identifying Children With Poor Cochlear Implantation Outcomes Using Massively Parallel Sequencing. *Medicine (Baltimore)* 94(27):e1073.
54. Kral A, Tillein J, Heid S, Klinke R, & Hartmann R (2006) Cochlear implants: cortical plasticity in congenital deprivation. *Prog Brain Res* 157:283-313.
55. Weible AP, *et al.* (2014) Perceptual gap detection is mediated by gap termination responses in auditory cortex. *Curr Biol* 24(13):1447-1455.
56. Aizenberg M, Mwilambwe-Tshilobo L, Briguglio JJ, Natan RG, & Geffen MN (2015) Bidirectional Regulation of Innate and Learned Behaviors That Rely on Frequency Discrimination by Cortical Inhibitory Neurons. *PLoS Biol* 13(12):e1002308.
57. Natan RG, *et al.* (2015) Complementary control of sensory adaptation by two types of cortical interneurons. *Elife* 4.
58. Michalski N & Petit C (2015) Genetics of auditory mechano-electrical transduction. *Pflugers Arch* 467(1):49-72.
59. Sahly I, *et al.* (2012) Localization of Usher 1 proteins to the photoreceptor calyceal processes, which are absent from mice. *J Cell Biol* 199(2):381-399.
60. Schietroma C, *et al.* (2017) Usher syndrome type 1-associated cadherins shape the photoreceptor outer segment. *J Cell Biol* 216(6):1849-1864.
61. Moller AR & Jannetta PJ (1983) Interpretation of brainstem auditory evoked potentials: results from intracranial recordings in humans. *Scand Audiol* 12(2):125-133.
62. Avan P, Buki B, & Petit C (2013) Auditory distortions: origins and functions. *Physiol Rev* 93(4):1563-1619.
63. Yagi H, *et al.* (2007) Vlgr1 is required for proper stereocilia maturation of cochlear hair cells. *Genes Cells* 12(2):235-250.
64. Lallemand Y, Luria V, Haffner-Krausz R, & Lonai P (1998) Maternally expressed PGK-Cre transgene as a tool for early and uniform activation of the Cre site-specific recombinase. *Transgenic Res* 7(2):105-112.
65. Ross KC & Coleman JR (2000) Developmental and genetic audiogenic seizure models: behavior and biological substrates. *Neurosci Biobehav Rev* 24(6):639-653.
66. Gavrieli Y, Sherman Y, & Ben-Sasson SA (1992) Identification of programmed cell death in situ via specific labeling of nuclear DNA fragmentation. *J Cell Biol* 119(3):493-501.
67. Paxinos G, Franklin KBJ, & Franklin KBJ (2001) *The mouse brain in stereotaxic coordinates* (Academic Press, San Diego) 2nd Ed.

Figures

Figure 1. Expression of *Cdhr23* and *Cdhr15* in MGE-derived interneuron precursors in the developing auditory cortex in mice

(*A*) Horizontal (upper panel) and coronal (lower panel) sections through the developing auditory cortex (AC) of wild-type E18.5 mouse embryos immunostained for cdhr23 and cdhr15. (*B*) Diagram of the migration routes of MGE-derived interneurons in the developing neocortex, and corresponding coronal sections of the AC of a *Nkx2.1*-cre*:Rosa*-tdTomato E18.5 mouse embryo immunostained for tdTomato and cdhr23 or cdhr15, with detailed views of tdTomato+ cdhr23+ or cdhr15+ interneurons (lower panel). (*C*) Coronal section of the AC of a wild-type E18.5 mouse embryo immunostained for cdhr23 and cdhr15. (*D*) Coronal section of the AC of a *Nkx2.1*-cre*:Rosa*-tdTomato P5 mouse immunostained for tdTomato and cdhr23 or cdhr15. Cell nuclei are stained in blue (DAPI). Abbreviations: H, hippocampus; A/S/I/OC, auditory/somatosensory/insular/orbital cortex; E/VC, entorhinal/visual cortex; (s)vz, (sub)ventricular zone; iz, intermediate zone; cp, cortical plate; mz, marginal zone; IN, interneuron; p, posterior; l, lateral; m, medial; d, dorsal.

Figure 2. Co-expression of *Cdhr23* and *Cdhr15* in MGE-derived postmitotic interneuron precursors in mice

(*A*) Diagram of the tangential migration routes of MGE-derived interneurons on a coronal section of the mouse embryonic telencephalon on E13.5-E15.5. (*B,C*) Coronal basal telencephalon sections of a *Nkx2.1*-cre*:Rosa*-tdTomato E13.5 embryo immunostained for tdTomato and cdhr23 (*B*) or cdhr15 (*C*), with detailed views of the MGE shown below. Note the expression of cdhr23 and cdhr15 in tdTomato+ neurons of the striatum and globus pallidus. (*D*) Coronal section of the MGE of a wild-type E13.5 embryo, immunostained for cdhr23 and MKI67, a cell proliferation marker. (*E*) Detailed view of the MGE of a wild-type E13.5 embryo immunostained for cdhr23 and cdhr15.

Abbreviations: NCx, neocortex; L/MGE, lateral/medial ganglionic eminence; POA, preoptic area; GP, globus pallidus; (s)vz, (sub)ventricular zone; iz, intermediate zone; cp, cortical plate; mz, marginal zone; l, lateral; m, medial; d, dorsal.

Figure 3. Abnormally small number of PV interneurons in the auditory cortex of mice with mutations of *Cdhr23* or *Cdhr15*

(*A, B*) Density of PV interneuron cell bodies in the auditory cortex (AC) of wild-type, *Cdhr23*$^{-/-}$ and *Cdhr15*$^{av\text{-}3J/av\text{-}3J}$ mice (*A*), and in the AC of *Cdhr23*$^{+/-}$ and *Cdhr15*$^{+/av\text{-}3J}$ mice with/without audiogenic seizures (AS+/AS- mice) on P27 (*B*); Coronal sections (upper panel), and detailed views (lower panel) are shown. Note that the remaining PV interneurons in *Cdhr23*$^{-/-}$ and *Cdhr15*$^{av\text{-}3J/av\text{-}3J}$ mice, and in *Cdhr23*$^{+/-}$ and *Cdhr15*$^{+/av\text{-}3J}$ mice with audiogenic seizures have a lower-density dendritic arborization than in wild-type mice. (*C*) Density of SST interneuron cell bodies in the AC of wild-type, *Cdhr23*$^{-/-}$ and *Cdhr15*$^{av\text{-}3J/av\text{-}3J}$ mice, and in the AC of *Cdhr23*$^{+/-}$ and *Cdhr15*$^{+/av\text{-}3J}$ AS+/AS- mice on P27; Coronal sections of the AC of wild-type, *Cdhr23*$^{-/-}$, and *Cdhr15*$^{av\text{-}3J/av\text{-}3J}$ P27 mice immunostained for PV and SST are shown. Note that the SST interneuron density was not linked to a susceptibility to audiogenic seizures ($P = 0.22$). (*D, E*) Density of PV interneuron cell bodies in the somatosensory (*D*) and motor cortices (*E*) of wild-type, *Cdhr23*$^{+/-}$ mice, and *Cdhr15*$^{+/av\text{-}3J}$ P27 mice; Coronal sections of the wild-type mice and *Cdhr23*$^{+/-}$ mice displaying audiogenic seizures immunostained for PV and SST. Abbreviations: H, hippocampus; AS+/AS- mice, mice with/without audiogenic seizures; d, dorsal; m, medial; l, lateral. Data are means ± s.e.m, with individual values (open circles). The number of mice analyzed for each genotype is indicated between brackets. **, $P < 10^{-2}$; ns, not significant (non-parametric two-tailed Mann-Whitney tests).

Figure 4. Abnormally small number of PV interneurons in the auditory cortex of mice with conditional deletion of *Cdhr23* or *Cdhr15* in MGE-derived interneuron precursors

(*A*) Coronal sections of the AC of *Nkx2.1*-cre*:Rosa*-tdTomato, *Cdhr23* cKO, and *Cdhr15* cKO mice on P27 immunostained for PV and tdTomato. (*B*) Bar graphs showing the density of cell bodies of PV interneurons, SST interneurons, and tdTomato+ interneurons that do not express PV or SST, in the AC of *Nkx2.1*-cre*:Rosa*-tdTomato, *Cdhr23* cKO, and *Cdhr15* cKO mice on P27. Abbreviations: d, dorsal; l, lateral. Data are means ± s.e.m, with individual values (open circles). The number of mice analyzed for each genotype is indicated between brackets. **, $P < 10^{-2}$; ns, not significant (non-parametric two-tailed Mann-Whitney tests).

Figure 5. *In situ* conditional deletion of *Cdhr15* in the AC of mice induces susceptibility to audiogenic seizures and reduced number of PV interneurons

(*A*) Coronal sections of the auditory cortex (AC) of wild-type and *Cdhr15*$^{lox/lox}$ P5 mice injected on P1 with the LV-*cre-GFP* recombinant virus, immunostained for cdhr23 and cdhr15. The site of injection is indicated on the diagram. (B) Detailed view of PV-immunoreactive interneurons in AC coronal sections from LV-*cre-GFP* P1-injected wild-type and *Cdhr15*$^{lox/lox}$ mice on P24. (*C*) Density of PV interneuron cell bodies in mice tested for susceptibility to audiogenic seizures. Abbreviations: AS+/AS- mice: mice with/without audiogenic seizures; d, dorsal; l, lateral. Data are individual values (open circles). **, $P < 10^{-2}$ (non-parametric two-tailed Mann-Whitney test).

Figure 6. Critical role of *Cdhr23* and *Cdhr15* in the migration of MGE-derived interneuron precursors

(*A*) Coronal section of the telencephalon in a *Nkx2.1*-cre*:Rosa*-tdTomato E15.5 mouse embryo, immunostained for tdTomato and cdhr23, and detailed view of the neocortex (lower panel). (*B*) Coronal sections of the telencephalon in wild-type, *Cdhr23*$^{-/-}$, and *Cdhr15*$^{-/-}$ E14.5 mouse embryos

immunostained for both cdhr23 and cdhr15, cdhr15, and cdhr23, respectively. (*C*) Representative neurons migrating from MGE explants of a wild-type mouse, cultured on a cdh2/laminin substrate, and immunostained for actin, cdhr23, and cdhr15 without permeabilization (left panel), or immunostained for actin and the centrosome marker γ-tubulin (arrowheads) after permeabilization (middle left panel). The histograms show the distribution of centrosome angular positions (see diagram) in unipolar cells, and the chart indicates the number of processes (one, two, or three) of cdhr15+ and cdhr23+ neurons derived from *Cdhr23*$^{-/-}$ and *Cdhr15*$^{-/-}$ MGE explants, cultured on cdh2/laminin substrate, respectively (right panels). Abbreviations: NCx, neocortex; L/MGE, lateral/medial ganglionic eminence; (s)vz, (sub)ventricular zone; iz, intermediate zone; cp, cortical plate; mz, marginal zone; d, dorsal; m, medial; c, centrosome; gc, growth cone. **, $P < 10^{-2}$; ***, $P < 10^{-3}$; ns, not significant (Kolmogorov-Smirnov tests for the centrosome angular position data, Chi squared test for the cell polarity data).

Figure 7. Defective development of MGE-derived cdhr23+/cdhr15+ GABAergic interneurons in *Adgrv1*$^{-/-}$ mice

(*A*) Coronal sections of the auditory cortex (AC) of *Adgrv1*$^{+/-}$ and *Adgrv1*$^{-/-}$ P27 mice immunostained for PV with detailed views (lower panels), and bar graph showing the density of PV interneuron cell bodies. (*B*) Coronal section of the AC of an *Adgrv1*$^{-/-}$ P27 mouse immunostained for PV and SST, and bar graph showing the density of SST interneuron cell bodies in wild-type and *Adgrv1*$^{-/-}$ mice. (*C*) Coronal section of the telencephalon of a *Nkx2.1*-cre*:Rosa*-tdTomato mouse embryo on E14.5, immunostained for tdTomato and adgrv1 and detailed view of the embryonic cortex (right panel). *(D)* Coronal sections of the telencephalon of *Adgrv1*$^{+/-}$ and *Adgrv1*$^{-/-}$ mouse embryos on E14.5, immunostained for cdhr23 and cdhr15. Abbreviations: NCx, neocortex; L/MGE, lateral/medial ganglionic eminence; (s)vz, (sub)ventricular zone; iz, intermediate zone; cp, cortical plate; mz, marginal zone; d, dorsal; m, medial; l: lateral. Data are means ± s.e.m with individual values (open

665 circles). The number of mice analyzed for each genotype is indicated between brackets. **, $P < 10^{-2}$;
666 ns, not significant (non-parametric two-tailed Mann-Whitney tests).
667
668 **Figure 8. Expression of *Cdhr23*, *Cdhr15* and *Adgrv1* in the MGE and developing auditory**
669 **cortex of macaque embryos**
670 (*A*) Coronal sections of the telencephalon in an E63 macaque embryo, immunostained for cdhr23,
671 cdhr15, or adgrv1. The MGE mantle zone is indicated by an asterisk and the MGE ventricular zone
672 by an arrow. The different regions are shown on the diagram. (*B*) Sagittal sections of the developing
673 auditory cortex (AC) of an E85 macaque embryo immunostained for Dlx5 and cdhr23, cdhr15, or
674 adgrv1 showing the outer subventricular zone and the subplate (see diagram of the brain cortical
675 layers on the left side). (*C*, *D*) High-magnification views of GABAergic interneuron precursors in the
676 outer subventricular zone, immunostained for Dlx5 and either cdhr23 or cdhr15 (*C*), and of a radial
677 glial cell immunostained for adgrv1 and nestin, a radial glia marker (*D*). Abbreviations: (s)vz,
678 (sub)ventricular zone; i/o svz, inner/outer svz; iz, intermediate zone; sp, subplate; cp, cortical plate;
679 mz, marginal zone; d, dorsal; m, medial; l, lateral.
680

Supporting Information

Auditory cortex interneuron development requires cadherins operating hair-cell mechanoelectrical transduction

Baptiste Libé-Philippot, Vincent Michel, Jacques Boutet de Monvel, Sébastien Le Gal, Typhaine Dupont, Paul Avan, Christine Métin[*], Nicolas Michalski[*] and Christine Petit[*,#].

* Joint senior authors

#Correspondence: christine.petit@pasteur.fr

I- Supplementary materials and methods

II- Legends to supplementary figures

Materials and methods

Animals. Animal experiments were performed in accordance with French and European regulations for the care and protection of laboratory animals (EC Directive 2010/63, French Law 2013-118, 6 February 2013), with authorization from the Institut Pasteur ethics committee for animal experimentation. *Adgrv1*^{tm1Msat} (*Adgrv1*$^{+/-}$ and *Adgrv1*$^{-/-}$) mice and *Nkx2.1*-cre mice were kindly provided by Makoto Sato (University of Fukui, Japan) (34, 63) and Nicoletta Kessaris (University College London, United Kingdom) (19), respectively. *Cdhr15*$^{av-3J}$ mice, which carry a point mutation resulting in a frameshift and premature stop codon, and *Rosa*-tdTomato mice were obtained from Jackson Laboratories (Bar Arbor, USA). *Cdhr23*$^{tm1.2Ugds}$ (*Cdhr23*$^{+/-}$ and *Cdhr23*$^{-/-}$) mice and *Cdhr23*$^{lox/lox}$ mice, in which lox P sites were introduced into the introns 61 and 68, have been described elsewhere (29). *Cdhr15*$^{ex5-fl}$ (*Cdhr15*$^{lox/lox}$) mice were generated by the Institut Clinique de la Souris (iCS, Illkirch, France). The targeting vector was constructed as follows. A 0.6 kb fragment encompassing exon 5 was amplified by PCR (from C57Bl/6N ES cells genomic DNA) and inserted into a proprietary iCS vector containing a LoxP site and a floxed and flipped neomycin resistance cassette. A 4.5 kb fragment (corresponding to the 5' homology arm) and a 2.8 kb fragment (corresponding to the 3' homology arm) were amplified by PCR and inserted into the vector obtained in the first step, to produce the final targeting construct. The targeting construct was introduced into C57Bl/6N embryonic stem (ES) cells by electroporation. Clones were selected and identified by PCR with external primers, and their identity was confirmed by Southern blot analysis with 5' and 3' external probes. Two recombinant ES clones were injected into BALB/cN blastocysts, to get male chimeras with germline transmission of the floxed allele. The *Cdhr15*$^{lox/lox}$ mice behaved like wild-type mice. *Cdhr15*$^{+/-}$ and *Cdhr15*$^{-/-}$ mice were obtained by crossing *Cdhr15*$^{lox/lox}$ mice with *PGK-cre* transgenic mice, in which *cre* expression is driven by the ubiquitously expressed early active promoter of the phosphoglycerate kinase-1 (PGK) gene (64). The mice had mixed genetic backgrounds combining C57BL/6JRj and SV/129, except for *Rosa*^{tdTomato} mice, which had a mixture

of C57BL/6JRj, SV/129, and Swiss backgrounds. The wild-type animals for lentiviral vector injections were C57BL/6JRj mice from Janvier Labs (Le Genest-Saint-Isle, France), whereas all other mice described as “wild-type” were littermates of the mutant mice.

Sound stimulation. We assessed susceptibility to audiogenic seizures by delivering continuous pure tones (from 5 kHz to 40 kHz) from a calibrated loudspeaker placed on top of a large Plexiglas cylinder (height: 30 cm; diameter: 15 cm) containing the freely moving mouse. Audiogenic seizures typically occurred as follows: the mice ran about wildly, then underwent tonico-clonic convulsions, tonic hyperextension of the hindlimbs, and a potentially fatal post-ictal depression of consciousness. Stimulation was stopped as soon as the animal began running about wildly, to prevent full-blown seizures (65). We evaluated the proportion of mice displaying audiogenic seizures in P21 to P35 mice, after stimulation with high-intensity (100-110 dB) pure tones (8-15 kHz) lasting up to one minute.

Injection of lentiviral vectors. Mice were anesthetized by hypothermia on P1, or with isoflurane (4% during induction, and then 2% through a mask during injection) on P10. We used a microinjector (Nanoliter 2000, World Precision Instruments, Sarasota, USA) to inject lentiviral vector (70 nL; *Pgk::cre-GFP or Pgk::GFP;* 10^7 TU/ml, Kerafast, Boston, USA) bilaterally into the temporal cortex to target the AC, or dorsally into the motor cortex.

Hearing tests. Mice were anesthetized by intraperitoneal xylazine (7.5 mg/kg) and ketamine (75 mg/kg) injections. Auditory brainstem responses (ABRs) (61) were recorded in response to pure tone bursts at frequencies of 5, 10, 15, 20, 32, and 40 kHz. Sound intensities between 15 dB and 115 dB SPL, in 5 dB steps, were tested. ABRs were averaged over 100-200 pure-tone stimulus presentations. ABR thresholds were defined as the lowest stimulus level resulting in recognizable waves. ABR

wave-I amplitude was estimated by measuring the voltage difference between the wave-I peak and the trough between wave-I and wave-II, and ABR wave-I latency was measured as the time from sound stimulation to the wave-I peak. Electrode responses were amplified (gain of 10 000), filtered, digitally converted, and averaged with a compressed-data acquisition system.

Distortion product otoacoustic emissions were collected with a miniature microphone at the entry to the ear canal (62). Two primary pure-tone stimuli of frequencies f_1 and f_2 were applied simultaneously: f_2 was set at different values between 5 and 20 kHz and the f_2/f_1 ratio was kept constant at 1.2. The cubic difference tone at $2f_1 - f_2$, the most prominent distortion product generated by mammalian ears, was measured for primary tone frequencies of equal intensity, from 40 to 75 dB SPL.

Tissue preparation. Cryopreserved brain sections from macaque (*Macaca fascicularis*) embryos (E63 and E85) were provided by Colette Dehay (PrimaLyon Platform, Institut Cellule Souche et Cerveau, INSERM, Bron, France). Midday vaginal plugs were considered to correspond to embryonic day 0.5 (E0.5), for staging purposes. Mouse embryos were dissected and fixed by immersion in 4% paraformaldehyde (PFA) in phosphate-buffered saline (PBS). Mouse pup brains were removed before embryo fixation in 4% PFA in PBS. At later stages, mice were deeply anesthetized with xylazine (60 mg/kg) and ketamine (150 mg/kg), by intraperitoneal injection, before intracardiac perfusion with 4% PFA in PBS. Mouse embryonic tissues were postfixed for three days in 4% PFA in PBS, and embedded in 2% agarose for free-floating vibratome slicing (50 µm sections) with a Leica VT1000S (Leica Biosystems, Wetzlar, Germany), or postfixed overnight in 4% PFA in PBS, protected by immersion in 30% sucrose, and embedded in optimal cutting temperature (OCT) compound (VWR International, Radnor, USA) for cryostat sectioning (20 µm sections). After P20, 50 µm thick free-floating cryosections were cut. Where appropriate, sections were processed on Superfrost Plus slides

(Menzel-Gläser, Braunschweig, Germany). Standard procedures were used to process samples for immunolabeling.

Immunolabeling. Sections were cut from prepared tissues, permeabilized and blocked in PBS supplemented with 0.25% Triton X-100 (Sigma-Aldrich) and 1% BSA (AppliChem, Darmstadt, Germany). The following primary antibodies were used: rabbit anti-adgrv1 antiserum against the N-terminal region (1:100; Fig. S1A; previously described (37)) for mouse experiments, and rabbit anti-adgrv1 polyclonal antibody directed against the C-terminal region (1:500; Fig. S1A; previously described (59)) for macaque experiments, rabbit anti-caspase-3 polyclonal antibody (1:500; #HPA002643, Sigma-Aldrich, Saint-Louis, USA), rabbit anti-cdhr23 polyclonal antibody against extracellular epitopes corresponding to extracellular cadherin repeat 11 (1:300; C1EC11, Fig. S1A; previously described (59)), rabbit anti-cdhr15 polyclonal antibody against the extracellular region next to the transmembrane domain (1:300; P1ExJM, Fig. S1A; previously described (59), Figs. 1A (coronal), 1B, 1D, 2C, 6A, 7B, 9, S2, S7B, S7C-E, S7F-G, S9), mouse anti-cdhr15 monoclonal antibody against extracellular epitopes corresponding to cadherin repeats 7 to 10 (1:300; #sc-377235, Fig. S1A; Santa Cruz Biotechnology, Dallas, USA; Figs. 1A (horizontal), 1C, 2E, 6C, 7D, S7A), rabbit anti-doublecortin polyclonal antibody (1:2000; #ab18723, Abcam, Cambridge, United Kingdom), mouse anti-Dlx5 monoclonal antibody (1:500; #SAB1412173, Sigma-Aldrich), chicken anti-GFP polyclonal antibody (1:1000; #ab13970, Abcam), mouse anti-nestin monoclonal antibody (1:1000; #556309, BD Biosciences, Franklin Lake, USA), rabbit anti-MKI67 polyclonal antibody (1:100; #ab15580, Abcam), mouse anti-PV monoclonal antibody (1:500; #SAB4200545, Sigma-Aldrich), rabbit anti-red fluorescent protein polyclonal antibody to detect tdTomato (1:2000; #3993-100, Clontech Laboratories, Mountain View, USA), rabbit anti-SST polyclonal antibody (1:250; #ab22682; Abcam), and mouse anti-γ-tubulin monoclonal antibody (1:500; #T6557; Sigma-Aldrich). The following secondary antibodies were used (1:500): goat anti-chicken Alexa Fluor 488-conjugated

antibodies (#A11039; Life Technologies, Waltham, USA), goat anti-mouse Alexa Fluor 488-conjugated (#A21121; Life Technologies), Atto550-conjugated (#43394; Sigma-Aldrich), and Atto647-conjugated (#50185; Sigma-Aldrich) antibodies, goat anti-rabbit Atto488-conjugated (#18772; Sigma-Aldrich), Atto550-conjugated (#43328; Sigma-Aldrich) and Atto647N-conjugated (#40839; Sigma-Aldrich) antibodies. The epitopes detected by rabbit anti-cdhr23, anti-cdhr15, and mouse anti-Dlx5 antibodies are conserved in the corresponding macaque proteins. The epitope detected by the adgrv1-Cter antibody in macaque is 93% identical to that in mouse. Rabbit anti-cdhr23, anti-cdhr15, and anti-adgrv1-Cter antibodies have already been used in macaque (59). The anti-nestin antibody has been shown to be reactive in primates (DSHB Hybridoma Bank). Actin filaments were stained with Atto-565-conjugated phalloidin (1:1000, #94072, Sigma-Aldrich). Nuclei were stained with 4',6-diamidino-2-phenylindole (DAPI) (1:7500, #D9542, Sigma-Aldrich). When two primary antibodies for proteins from the same species were used, the same protocol was used, but in two steps (37): staining for one marker only, fixing of the samples in 4% PFA in PBS for 30 minutes, three washes, and then staining for the other marker. Apoptosis was assessed in TUNEL (terminal deoxynucleotidyl transferase dUTP nick-end labeling) assays (Roche, West Sussex, UK) (66).

Samples were mounted in Fluorsave (Calbiochem, San Diego, USA). Images were captured with an LSM-700 confocal microscope (Zeiss, Oberkochen, Germany) with a 63x NA 1.4 Plan Apochromatic oil immersion objective, a 25x NA 0.8 LCI Plan Neofluar objective, a 5x NA 0.16 Plan Apochromatic non-immersion objective, or a 20x NA 0.8 Plan Apochromatic non-immersion objective, or with a MVX10 macroscope (Olympus Tokyo, Japan). All images were converted to RGB format with ImageJ (NIH, Bethesda, USA) and processed with Photoshop (Adobe, San José, USA). The images in Figs. 1A, 2B-C, 3A-B (large views), 6A-B, 6C (cdhr23/cdhr15 staining), 7A (large view), 7C-D, 8, S2B-D, S4, S6A, S7A, S8B (detailed views), S9 are single focal sections. The images in Figs. 1B-D, 2D-E, 3A & 3B (detailed views), 3B-E, 4, 5A-B, 6C (γ-tubulin staining), 7A

(detailed view), 7B, S2A, S5, S6B, S7B, S7C-E, S8A, S8B (large views) are mean projected Z-stacks.

Quantification of staining on histological sections. The boundaries of the AC, including the auditory core and belt areas, were determined based on the mouse brain atlas (67). For each animal, five to six coronal sections (60 µm thick) spanning the anterior-posterior axis of the auditory cortex were imaged bilaterally. Cdhr23+/cdhr15+ tdTomato+, PV or SST interneuron cell bodies were quantified with the spot detector tool (bright spots on a dark background; sensitivity: 100%) of Icy software (Institut Pasteur, Paris, France). Only cell bodies with diameters exceeding 10 µm were considered. The total number of cell bodies was then normalized by the total surface considered, to obtain a PV interneuron density for each animal. For each animal, the thickness of the AC was quantified on five successive coronal sections (60 µm thick) and then averaged. Surface of the AC was estimated on 5 sections (60 µm thick) spanning the anterior-posterior axis of the AC. The surface was then normalized for each animal by the total number of slices. Cortical thickness and surface of the AC were quantified using the Icy software onto the DAPI channel. Mean fluorescence on E14.5 sections was measured with ImageJ, comparing regions of interest in the subpallium and adjacent embryonic cortex.

Culture of MGE explants and quantification of migration. Sterile glass coverslips were coated with polylysine/laminin (Poly L Lysine hydrobromide #P1524, Sigma-Aldrich; laminin #L2020, Sigma-Aldrich) or polylysine/laminin/cdh2, as previously described (32). The cdh2 substrate was prepared from a cdh2-h-Fc chimera (#6626-NC-050, Bio-Techne, Minneapolis, USA). Each MGE from E13.5 embryos was dissected into nine explants, placed on the substrate, and cultured for 19 hours on laminin or 24 hours on cdh2/laminin in DMEM-F12 (#31331028, Fisher Scientific, Waltham, USA) supplemented with 37% glucose (#G7021, Sigma-Aldrich), 2% B27 (#17504044, Fisher Scientific),

1% N2 (#17502048, Fisher Scientific), 1% Glutamax, and 20 U/mL penicillin/streptomycin (#15140122, Fisher Scientific). The MGE explants were fixed by incubation in 4% PFA in 0.33 M sucrose phosphate buffer for 24 hours, and processed by standard immunohistochemistry procedures, as described above. In one case (see Fig. 6C), cultured neurons were left unpermeabilized for studies of the extracellular distribution of cdhr23 and cdhr15 only.

We characterized potential differences in migration pattern between mutant neurons lacking cdhr23 or cdhr15 and wild-type neurons, by considering a subpopulation of MGE neurons sufficiently isolated from the colony after migrating away from the explant. We analyzed the geometric characteristics of the processes and growth cones of the selected neurons, and manually segmented them on the maximum-projected confocal stacks, using a customized Matlab interface. The segmentation process involved a spline-curve delineation of relevant structures, including the cell nucleus and processes. A neuronal process was defined as any process emanating from the cell body and terminating in a growth cone. Any other processes (e.g., branching from a leading process or not terminating in a growth cone) were discarded. We measured the vector running from the centrosome to the center of the cell nucleus, and the angle of this vector relative to the axis of the leading process in unipolar cells.

The migration area (surrounding the explant, excluding the explant itself) was measured with Icy software. For cultures on laminin, the migration areas of the nine explants from a given MGE were summed. For cultures on cdh2/laminin, the three explants with the largest migration areas from the nine explants tested for a given MGE were considered as individuals. In this case, the migration area was quantified as the actin-labeled area: 1.67 ± 0.33 mm² (n = 17 explants) for the wild-type, 1.35 ± 0.20 mm² (n = 9 explants) for *Cdhr23*$^{-/-}$, and 1.90 ± 0.54 (n = 27 explants) for *Cdhr15*$^{-/-}$ explants ($P > 0.4$ for both comparisons between wild-type and mutant explants).

Statistical analysis. Data are expressed as the mean ± standard error of the mean (s.e.m). Unless otherwise stated, numbers (*n*) in the figures and text are the numbers of biological replicates derived from independent biological samples (individual animals). The animals in each experimental group originated from at least two independent mouse litters. Immunolabeling was performed on at least three animals in each case. The data were analyzed with Igor Pro (WaveMetrics), Prism (Graphpad), and the BiostaTGV webtool of R software (Institut Pierre Louis d'Epidémiologie et de Santé Publique, INSERM, UPMC, Paris, France). Non-parametric two-tailed Mann-Whitney tests were used to compare unpaired groups. Proportions of mice were compared in Chi squared tests (with Yates' correction) or Fisher's exact tests, depending on sample size. The association between susceptibility to audiogenic seizures and the smaller numbers of AC PV interneurons in grouped *Cdhr23*$^{+/-}$ and *Cdhr15*$^{+/av\text{-}3J}$ individuals was assessed in Mann-Whitney tests, after ANOVA for the genotype factor. The distributions of centrosome angular position were compared in Kolmogorov-Smirnov tests. Differences were considered statistically significant if $P < 0.05$. Asterisks on bar graphs indicate the statistical significance of the differences indicated in brackets (*, $P < 0.05$; **, $P < 10^{-2}$; and ***, $P < 10^{-3}$), whereas ns denotes "not significant" ($P > 0.05$).

Supporting Information legends

Supporting Information 1. Cadherin-related proteins of hair cell mechanoelectrical transduction are critically involved in the migration of a population of MGE-derived GABAergic interneuron precursors to the auditory cortex

(*A*) Protein domains of cdhr23, cdhr15, and adgrv1. The positions of the epitopes targeted by the antibodies used in the study are indicated by open boxes. (*B*) Diagram of the cochlea sensory epithelium showing the inner and outer hair cells (upper panel), and diagram of the hair bundles of mouse auditory hair cells between postnatal day 2 (P2) and P9. Cdhr23 and cdhr15 make up the tip-links that gate the mecahnoelectrical transduction channels, form transient lateral links between stereocilia, and form kinocilial links between the kinocilium and adjacent stereocilia of the tall row. Adgrv1 forms transient lateral links located at the base of the stereocilia (ankle links). Of those, only the tip-links remain in mature hair bundles. In the mouse auditory hair cells, the kinocilium disappears by P9. (*C*) Diagram showing the migration pathway of a population of embryonic MGE-derived interneuron precursors co-expressing *Cdhr23* and *Cdhr15*, specifically targeted to the auditory cortex (upper panel), and the defects observed in the migration of *Cdhr15*-expressing and *Cdhr23*-expressing interneuron precursors in *Cdhr23*$^{-/-}$ mice and *Cdhr15*$^{-/-}$ mice, respectively (lower panel). (D) Diagram showing the specific loss of parvalbumin (PV) interneurons in the auditory cortex of *Cdhr23*$^{-/-}$ or *Cdhr15*$^{-/-}$ P27 mice. Abbreviations: l, lateral; m, medial; d, dorsal; NCx, neocortex; L/MGE, lateral/medial ganglionic eminence; (s)vz, (sub)ventricular zone; iz, intermediate zone; cp, cortical plate; mz, marginal zone; E13.5-E15.5, embryonic days 13.5-15.5.

Supporting Information 2. Validation of the specificity of the antibodies directed against cdhr23, cdhr15, and adgrv1 on sections of the telencephalon of *Cdhr23*$^{-/-}$, *Cdhr15*$^{-/-}$, and *Adgrv1*$^{-/-}$ embryos, respectively

(*A*) Coronal section of the AC of a wild-type P7 mouse, immunostained for cdhr23 and cdhr15. (*B*) Coronal sections of the telencephalon of a wild-type E12.5 mouse embryo, immunostained for cdhr23, cdhr15, or adgrv1. (*C*) Coronal sections of the telencephalon of *Cdhr23*$^{-/-}$, *Cdhr15*$^{-/-}$, and *Adgrv1*$^{-/-}$ E14.5 mouse embryos, immunostained for cdhr23, cdhr15, and adgrv1, respectively. (*D*) Coronal sections of wild-type E15.5 mouse embryos, immunostained for cdhr23 or cdhr15. Abbreviations: NCx, neocortex; C/L/MGE, caudal/lateral/medial ganglionic eminence; POA, preoptic area; m, medial; d, dorsal.

Supporting Information 3. *Cdhr23*$^{+/-}$ and *Cdhr15*$^{+/av\text{-}3J}$ mice have normal auditory brainstem responses (ABRs) and distortion product otoacoustic emissions (DPOAEs)

ABR thresholds, ABR wave-I amplitude, ABR wave-I latency, and level of $2f_1$-f_2 DPOAE recorded for f_1 = 8.3 kHz and f_2 = 10 kHz, in *Cdhr23*$^{+/-}$ (*A*) and *Cdhr15*$^{+/av\text{-}3J}$ (*B*) mice. Data are means ± s.e.m with individual values (open circles). ns, not significant (non-parametric two-tailed Mann-Whitney tests).

Supporting Information 4. PV interneuron defects in *Cdhr23* cKO and *Cdhr15* cKO mice are restricted to the AC

Coronal sections of the telencephalon of *Nkx2.1*-cre:*Rosa*-tdTomato, *Cdhr23* cKO, and *Cdhr15* cKO P27 mice. Abbreviations: d, dorsal; m, medial; AC, auditory cortex; VC, visual cortex; TeA, temporal association cortex; H, hippocampus.

Supporting Information 5. Characterization of LV-*cre-GFP*-injected wild-type and *Cdhr15*$^{lox/lox}$ mice

(*A*) ABR thresholds in LV-*cre-GFP* P1-injected wild-type and *Cdhr15*$^{lox/lox}$ mice on P24. (*B*) Coronal sections of the auditory cortex (AC) of LV-*cre-GFP* P1-injected wild-type and *Cdhr15*$^{lox/lox}$ P5 mice, immunostained for GFP and caspase-3, a protein involved in cell apoptosis (left panel), and detailed view of cortical layer IV immunostained for GFP, caspase-3, and Dlx5, a GABAergic interneuron marker (right panel). Data are means ± SEM. ns, not significant (non-parametric two-tailed Mann-Whitney test).

Supporting Information 6. Preservation of the main tangential migration stream of neurons in *Cdhr23*$^{-/-}$ and *Cdhr15*$^{-/-}$ mouse embryos

(*A*) Coronal sections of the basal telencephalon of wild-type, *Cdhr23*$^{-/-}$, and *Cdhr15*$^{-/-}$ E14.5 mice, labeled by the TUNEL method. (*B*) Coronal sections of the telencephalon of wild-type, *Cdhr23*$^{-/-}$, and *Cdhr15*$^{-/-}$ E14.5 embryos, immunostained for the neuron migration marker doublecortin. Abbreviations: d, dorsal; m, medial; L/MGE, lateral/medial ganglionic eminence; NCx, neocortex; H, hippocampus; (s)vz, (sub)ventricular zone; iz, intermediate zone; cp, cortical plate; mz, marginal zone.

Supporting Information 7. Expression of *Cdhr23* and *Cdhr15* in neurons migrating from MGE explants of wild-type, *Cdhr23*$^{-/-}$, and *Cdrh15*$^{-/-}$ mouse embryos

(*A*) Coronal section of the telencephalon of a *Nkx2.1*-cre*:Rosa*-tdTomato E15.5 mouse embryo, immunostained for tdTomato and cdhr15 (upper panel), and detailed view of the neocortex (lower panel). (*B, C*) Representative MGE explants from wild-type, *Cdhr23*$^{-/-}$, and *Cdhr15*$^{-/-}$ E13.5 embryos cultured for 24 hours on a laminin substrate, with quantification of the migration area (*B*), or cultured for 19 hours on a cdh2/laminin substrate (C) with magnifications of migrating neurons

immunostained for cdhr23 or cdhr15 and actin (lower panel), and quantification of the migration area of neurons expressing cdhr23/cdhr15 relative to the area positive for actin. (*D, E*) Representative isolated neurons migrating from cultures of MGE explants of wild-type, *Cdhr23*$^{-/-}$ (*D*), and *Cdrh15*$^{-/-}$ (*E*) mouse embryos, cultured on a cdh2/laminin substrate, and immunostained for cdhr23, cdhr15, and actin. Cell nuclei are stained in blue (DAPI). Abbreviations: L/MGE, lateral/medial ganglionic eminence; NCx, neocortex; (s)vz, (sub)ventricular zone; iz, intermediate zone; cp, cortical plate; mz, marginal zone. Data are means ± s.e.m with individual values (open circles). The number of MGEs (*B*) and explants (*C*) analyzed for each genotype is indicated between brackets. **, $p < 0.01$; ns, not significant (non-parametric two-tailed Mann-Whitney tests).

Supporting Information 8. *Adgrv1* is expressed in MGE progenitor cells and auditory cortex radial glia cells

(*A*) Detailed view of the MGE in a wild-type E13.5 mouse embryo, immunostained for adgrv1 and MKI67. Note the adgrv1 labeling of the interneuron/glial cell progenitors in the proliferative zones. (*B*) Coronal section of the developing auditory cortex of a *Nkx2.1*-cre*:Rosa*-tdTomato E18.5 mouse embryo, immunostained for tdTomato, and adgrv1, with a high-magnification view of a tdTomato+ interneuron (*B*, left panel), and for adgrv1 and nestin, a radial glial marker, with a high magnification of the intermediate zone (*B*, right panel). Cell nuclei are stained in blue (DAPI). Abbreviations: (s)vz, (sub)ventricular zone; d, dorsal; m, medial; l, lateral.

Supporting Information 9. Expression of *Cdhr23*, *Cdhr15* and *Adgrv1* in the developing auditory cortex of macaque embryos

Sagittal sections of the auditory cortex (AC) of an E85 macaque embryo immunostained for cdhr23, cdhr15 or adgrv1. The positions of the different cortical layers are shown on the left side diagram.

Abbreviations: (s)vz, (sub)ventricular zone; i/o svz, inner/outer svz; iz, intermediate zone; sp, subplate; cp, cortical plate; mz, marginal zone; d, dorsal; l, lateral.

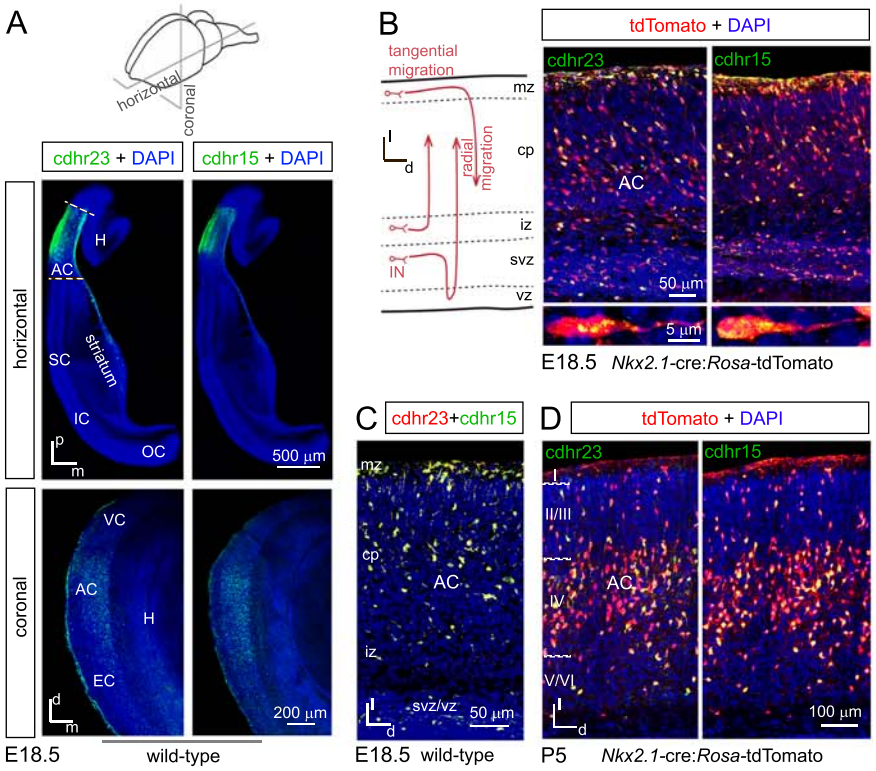
A
horizontal
coronal
cdhr23 + DAPI
cdhr15 + DAPI
horizontal
H
AC
striatum
SC
IC
OC
p
m
500 µm
coronal
VC
AC
H
EC
d
m
200 µm
E18.5
wild-type
B
tdTomato + DAPI
tangential migration
mz
cp
radial migration
iz
svz
IN
vz
d
cdhr23
cdhr15
AC
50 µm
5 µm
E18.5 Nkx2.1-cre:Rosa-tdTomato
C
cdhr23+cdhr15
mz
cp
AC
iz
svz/vz
50 µm
d
E18.5 wild-type
D
tdTomato + DAPI
cdhr23
cdhr15
I
II/III
IV
AC
V/VI
d
100 µm
P5 Nkx2.1-cre:Rosa-tdTomato

Figure 1

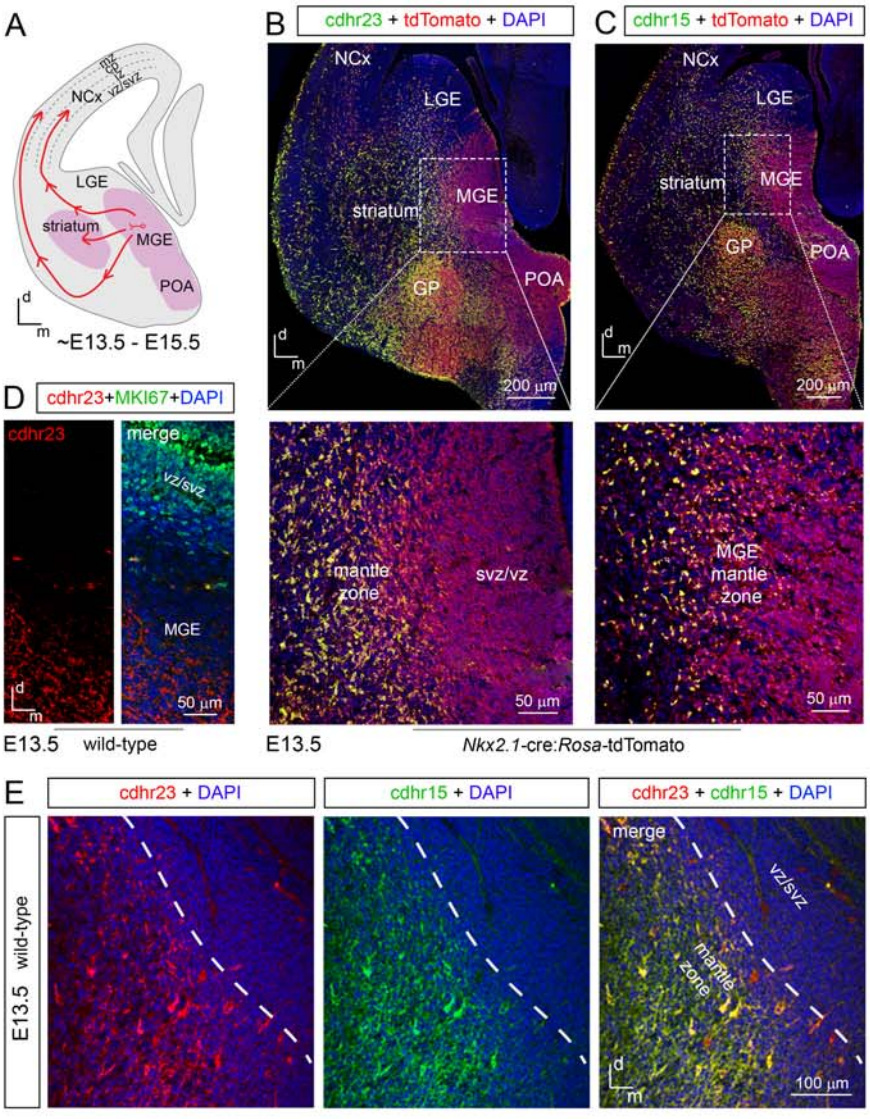
A
NCx
vz/svz
LGE
striatum
MGE
POA
d
m
~E13.5 - E15.5
B
cdhr23 + tdTomato + DAPI
NCx
LGE
striatum
MGE
GP
POA
200 µm
C
cdhr15 + tdTomato + DAPI
NCx
LGE
striatum
MGE
GP
POA
200 µm
D
cdhr23+MKI67+DAPI
cdhr23
merge
vz/svz
MGE
50 µm
mantle zone
svz/vz
50 µm
MGE mantle zone
50 µm
E13.5 wild-type
E13.5 Nkx2.1-cre:Rosa-tdTomato
E
cdhr23 + DAPI
cdhr15 + DAPI
cdhr23 + cdhr15 + DAPI
E13.5 wild-type
merge
vz/svz
mantle zone
100 µm

Figure 2

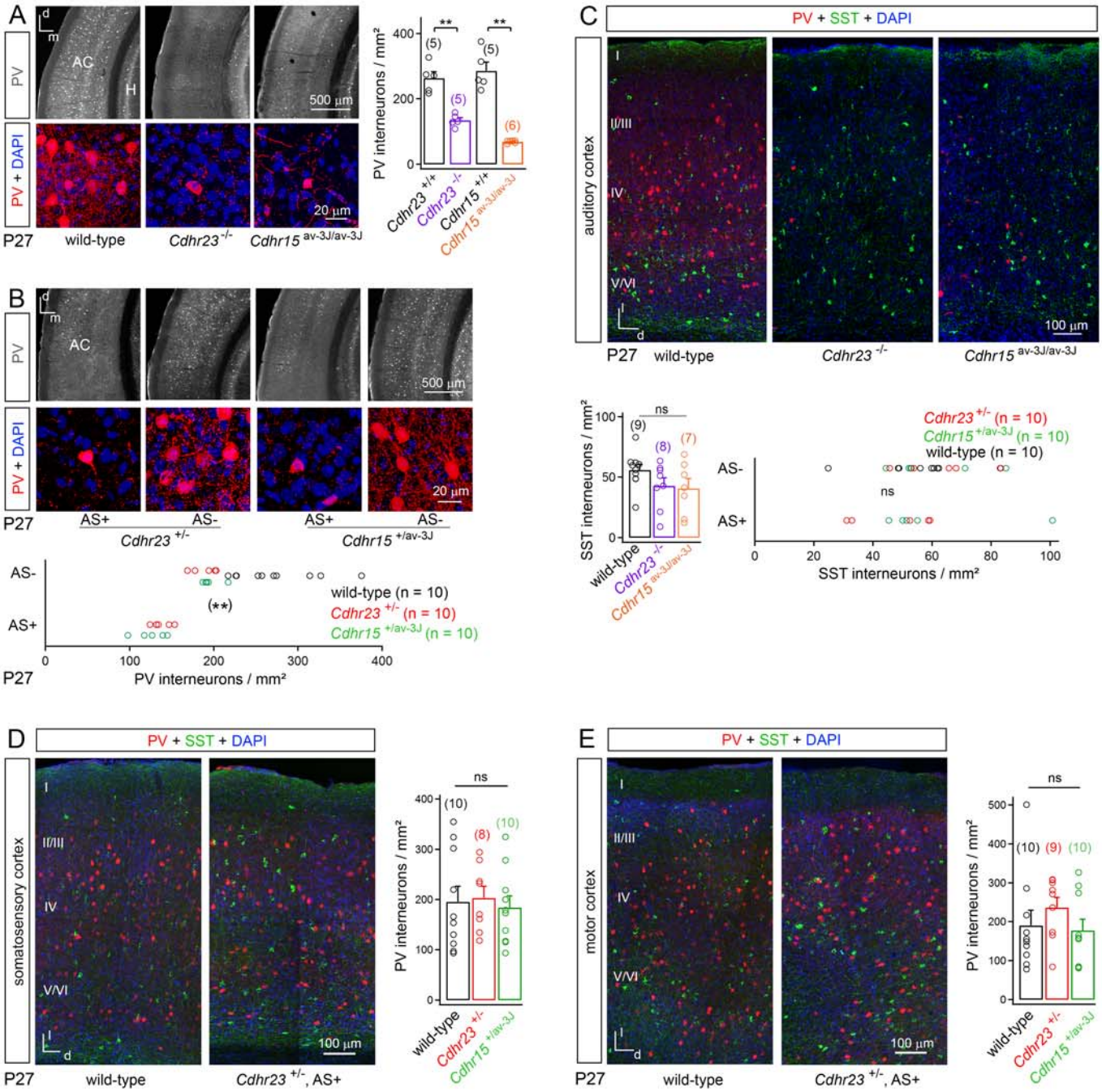
A
PV
PV + DAPI
AC
H
500 µm
20 µm
P27
wild-type
Cdhr23 -/-
Cdhr15 av-3J/av-3J
PV interneurons / mm²
**
(5)
(6)
Cdhr23 +/+
Cdhr23 -/-
Cdhr15 +/+
Cdhr15 av-3J/av-3J
B
AS+
AS-
Cdhr23 +/-
Cdhr15 +/av-3J
(**)
wild-type (n = 10)
Cdhr23 +/- (n = 10)
Cdhr15 +/av-3J (n = 10)
C
PV + SST + DAPI
auditory cortex
I
II/III
IV
V/VI
100 µm
ns
(9)
(8)
(7)
SST interneurons / mm²
D
somatosensory cortex
Cdhr23 +/-, AS+
(10)
E
motor cortex

Figure 3

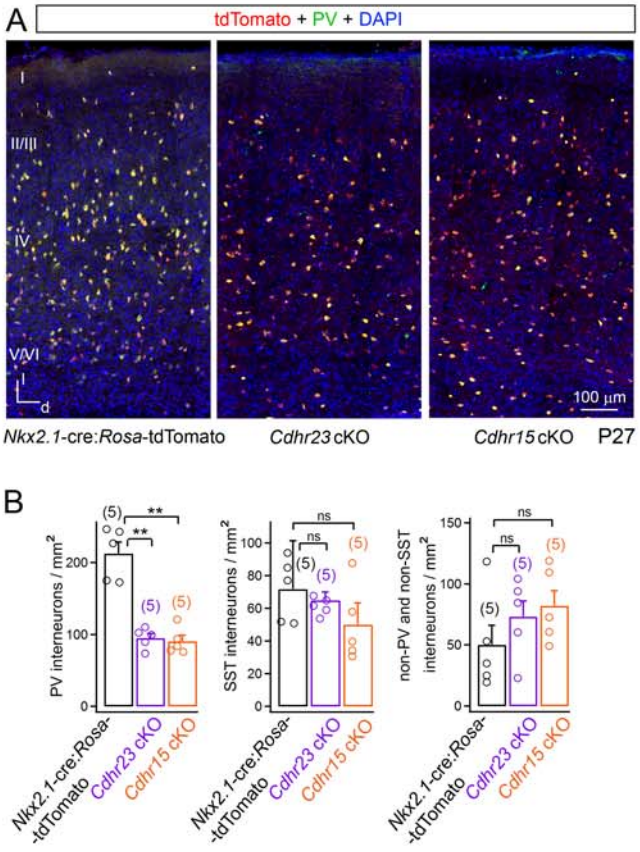
A
tdTomato + PV + DAPI
I
II/III
IV
V/VI
l
d
100 µm
Nkx2.1-cre:Rosa-tdTomato
Cdhr23 cKO
Cdhr15 cKO
P27
B
PV interneurons / mm²
SST interneurons / mm²
non-PV and non-SST interneurons / mm²
(5)
**
ns
Nkx2.1-cre:Rosa-tdTomato
Cdhr23 cKO
Cdhr15 cKO

Figure 4

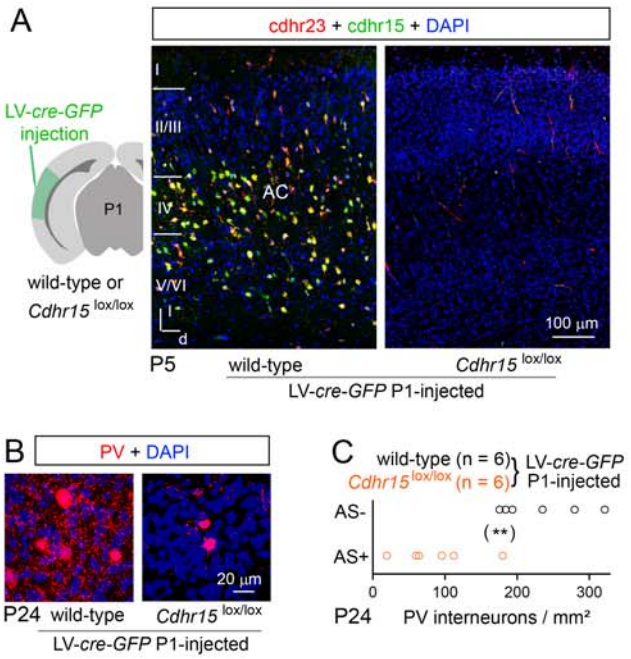
A
cdhr23 + cdhr15 + DAPI
LV-cre-GFP injection
P1
wild-type or Cdhr15 lox/lox
I
II/III
IV
AC
V/VI
l
d
100 µm
P5
wild-type
Cdhr15 lox/lox
LV-cre-GFP P1-injected
B
PV + DAPI
20 µm
P24 wild-type
Cdhr15 lox/lox
LV-cre-GFP P1-injected
C
wild-type (n = 6)
Cdhr15 lox/lox (n = 6)
LV-cre-GFP P1-injected
AS-
AS+
(**)
0
100
200
300
P24
PV interneurons / mm²

Figure 5

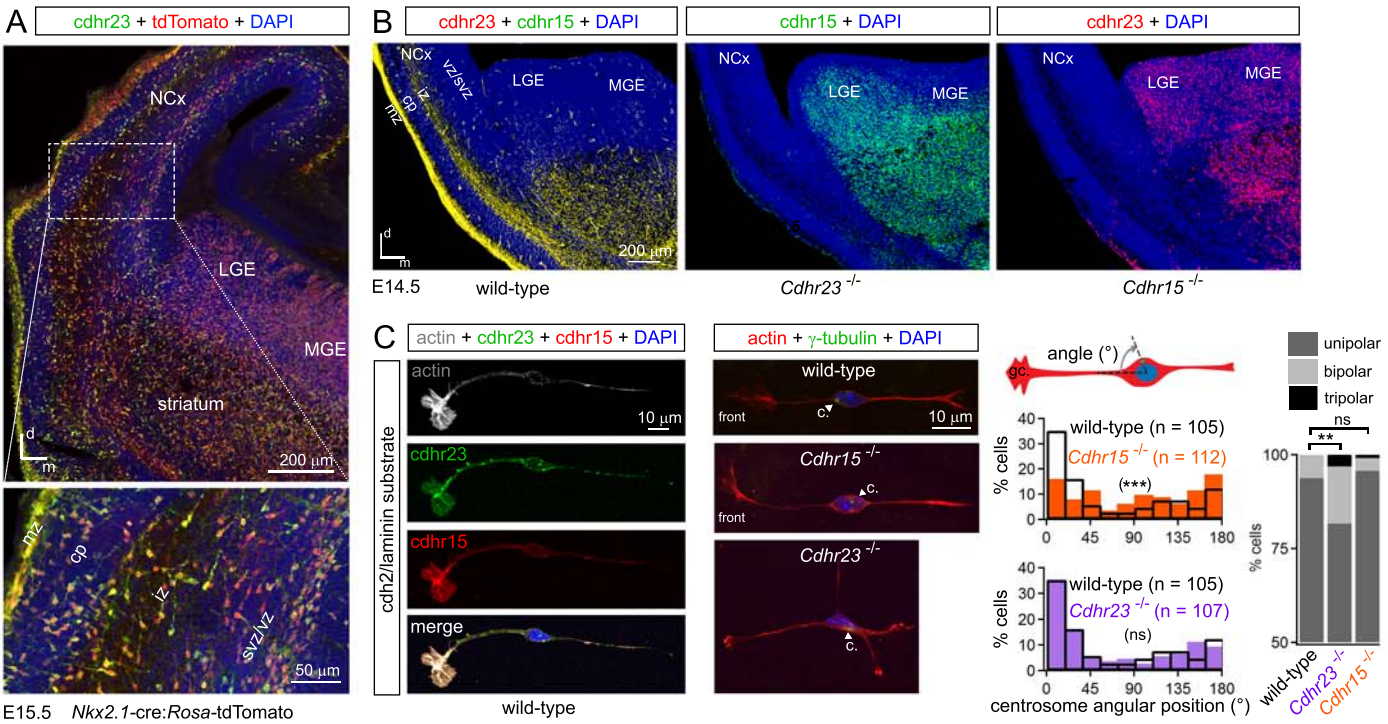
A
cdhr23 + tdTomato + DAPI
NCx
LGE
MGE
striatum
d
m
200 µm
mz
cp
iz
svz/vz
50 µm
E15.5 Nkx2.1-cre:Rosa-tdTomato
B
cdhr23 + cdhr15 + DAPI
cdhr15 + DAPI
cdhr23 + DAPI
NCx
LGE
MGE
vz/svz
iz
cp
mz
200 µm
E14.5 wild-type
Cdhr23 -/-
Cdhr15 -/-
C
actin + cdhr23 + cdhr15 + DAPI
cdh2/laminin substrate
actin
cdhr23
cdhr15
merge
10 µm
wild-type
actin + γ-tubulin + DAPI
wild-type
front
c.
10 µm
Cdhr15 -/-
Cdhr23 -/-
angle (°)
gc.
wild-type (n = 105)
Cdhr15 -/- (n = 112)
(***)
% cells
centrosome angular position (°)
Cdhr23 -/- (n = 107)
(ns)
unipolar
bipolar
tripolar
ns
**
wild-type
Cdhr23 -/-
Cdhr15 -/-

Figure 6

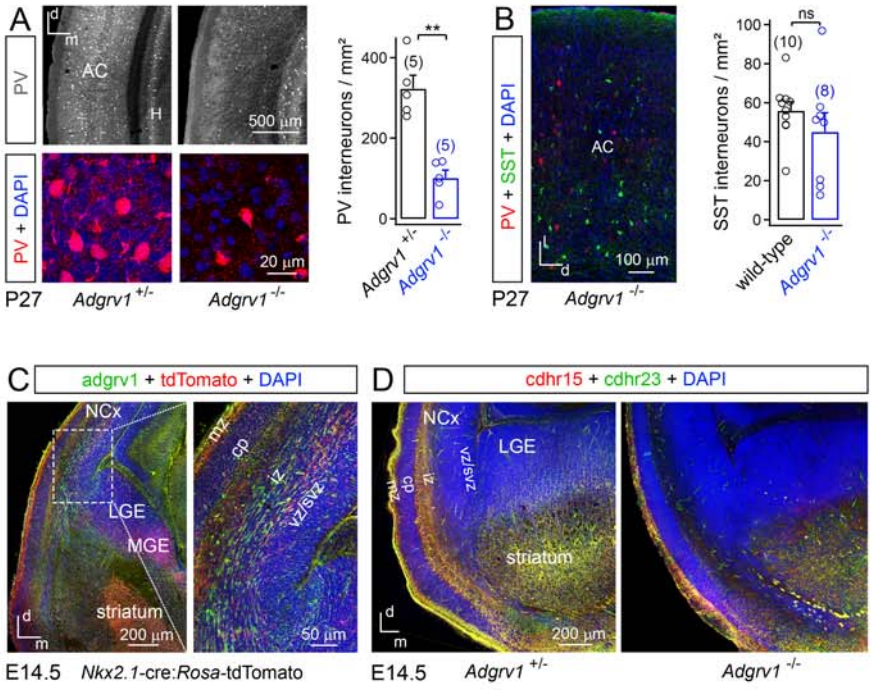
A
PV
PV + DAPI
d
m
AC
H
500 µm
20 µm
P27
Adgrv1 +/-
Adgrv1 -/-
PV interneurons / mm²
400
200
0
(5)
(5)
**
Adgrv1 +/-
Adgrv1 -/-
B
PV + SST + DAPI
AC
100 µm
P27
Adgrv1 -/-
SST interneurons / mm²
100
80
60
40
20
0
(10)
(8)
ns
wild-type
Adgrv1 -/-
C
adgrv1 + tdTomato + DAPI
NCx
LGE
MGE
striatum
200 µm
mz
cp
iz
zasvz
50 µm
E14.5
Nkx2.1-cre:Rosa-tdTomato
D
cdhr15 + cdhr23 + DAPI
NCx
LGE
vzsvz
striatum
200 µm
E14.5
Adgrv1 +/-
Adgrv1 -/-

Figure 7

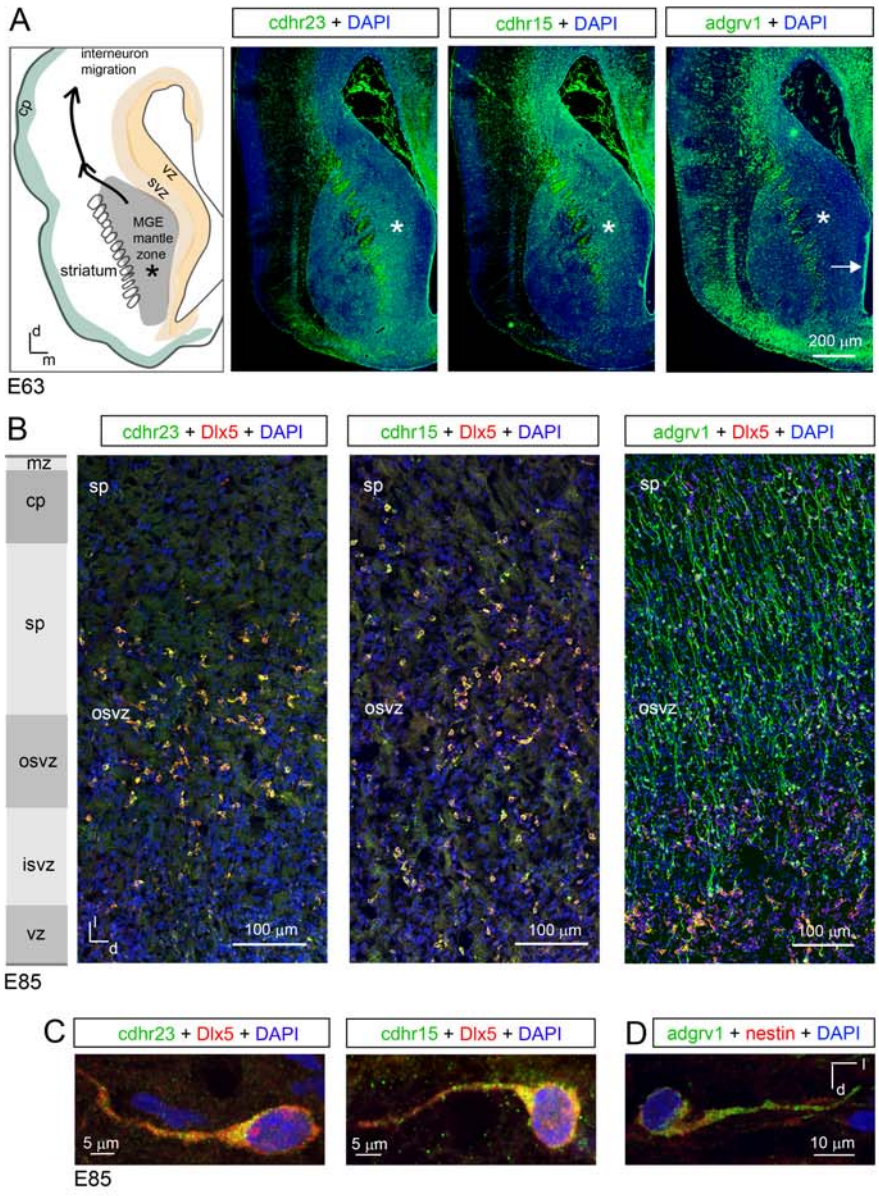
A
cdhr23 + DAPI
cdhr15 + DAPI
adgrv1 + DAPI
interneuron migration
cp
vz
svz
MGE mantle zone
striatum
d
m
200 µm
E63
B
cdhr23 + Dlx5 + DAPI
cdhr15 + Dlx5 + DAPI
adgrv1 + Dlx5 + DAPI
mz
cp
sp
osvz
isvz
vz
100 µm
E85
C
cdhr23 + Dlx5 + DAPI
cdhr15 + Dlx5 + DAPI
5 µm
D
adgrv1 + nestin + DAPI
10 µm
E85

Figure 8

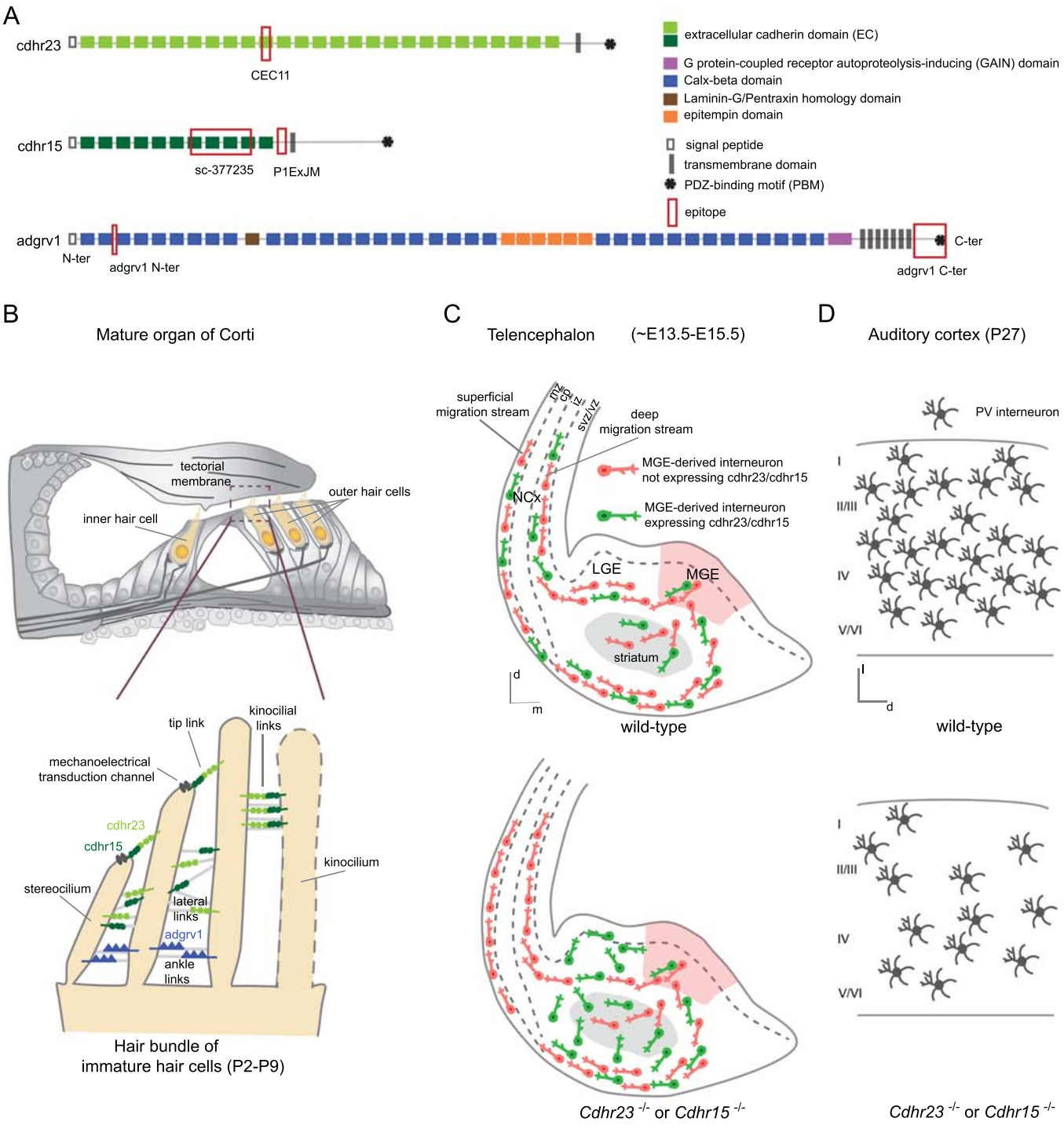

Supporting Information 1

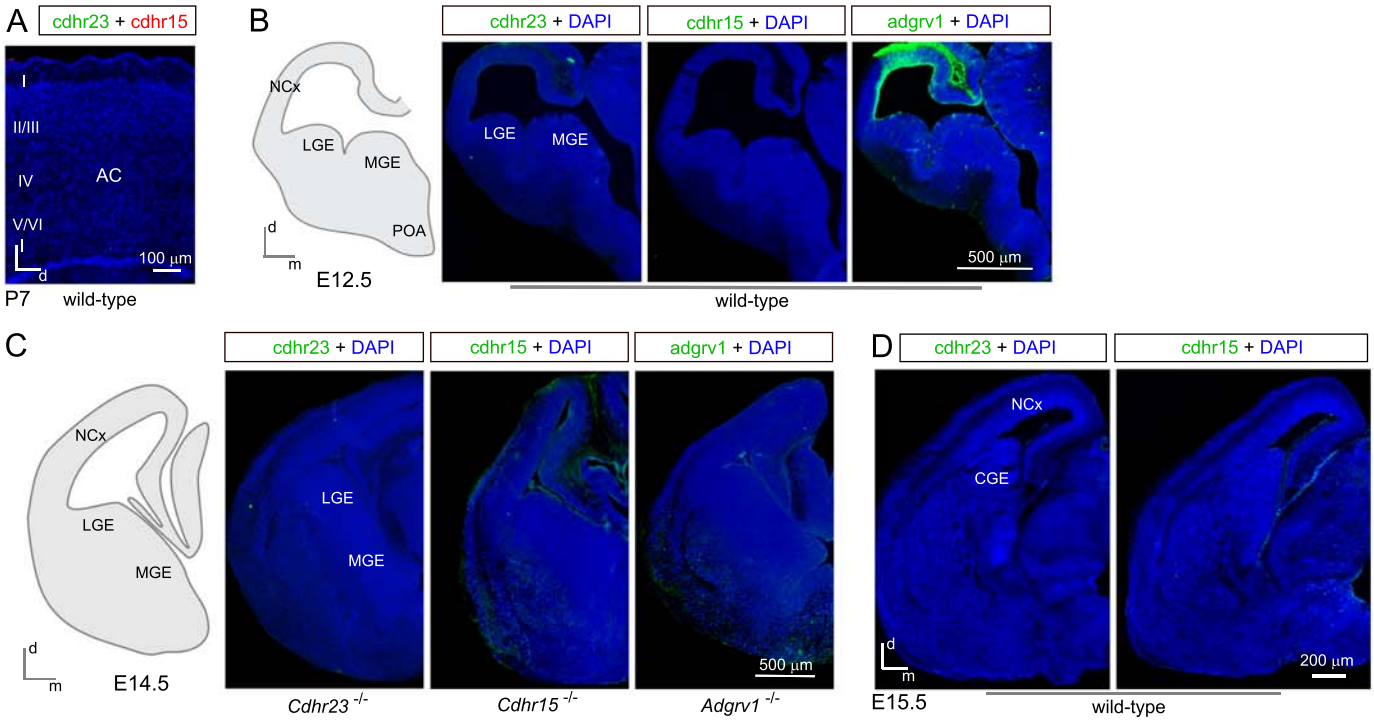

Supporting Information 2

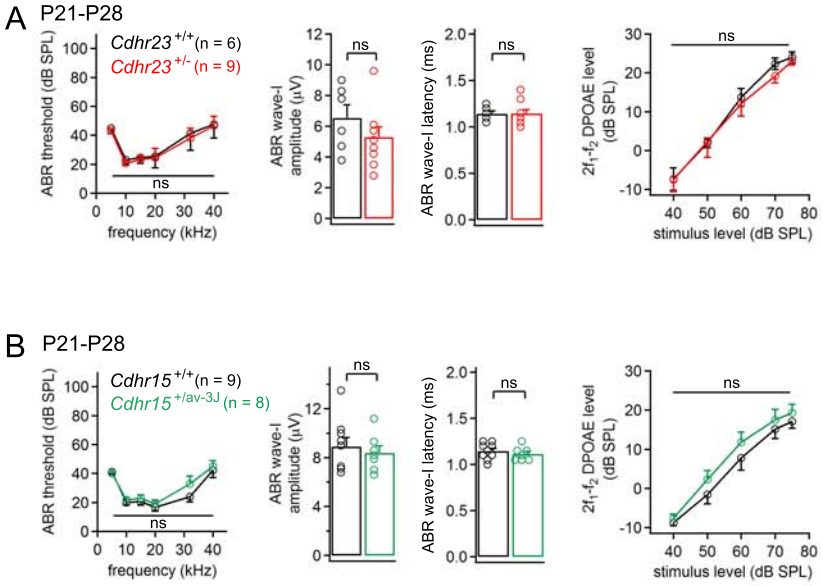

Supporting Information 3

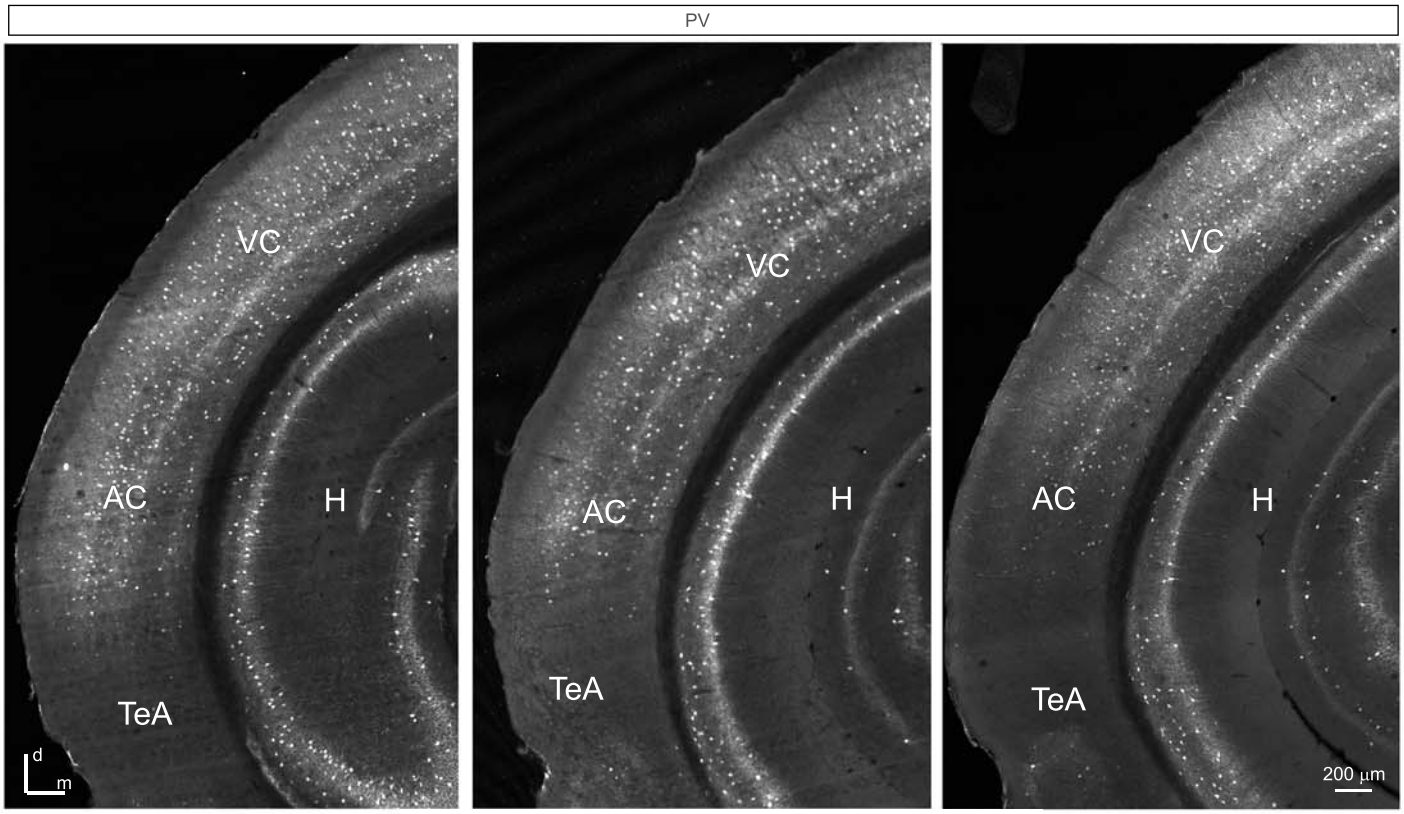

P27 *Nkx2.1*-cre:*Rosa*-tdTomato *Cdhr23* cKO *Cdhr15* cKO

Supporting Information 4

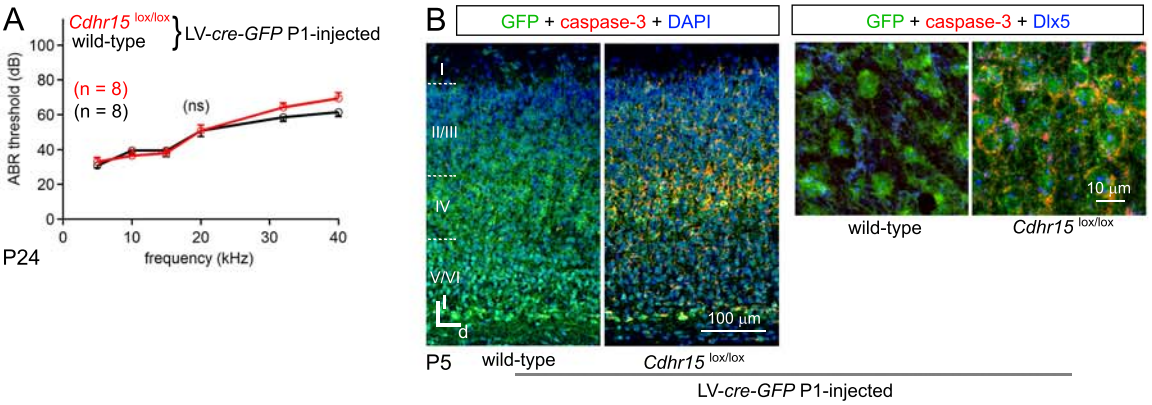

Supporting Information 5

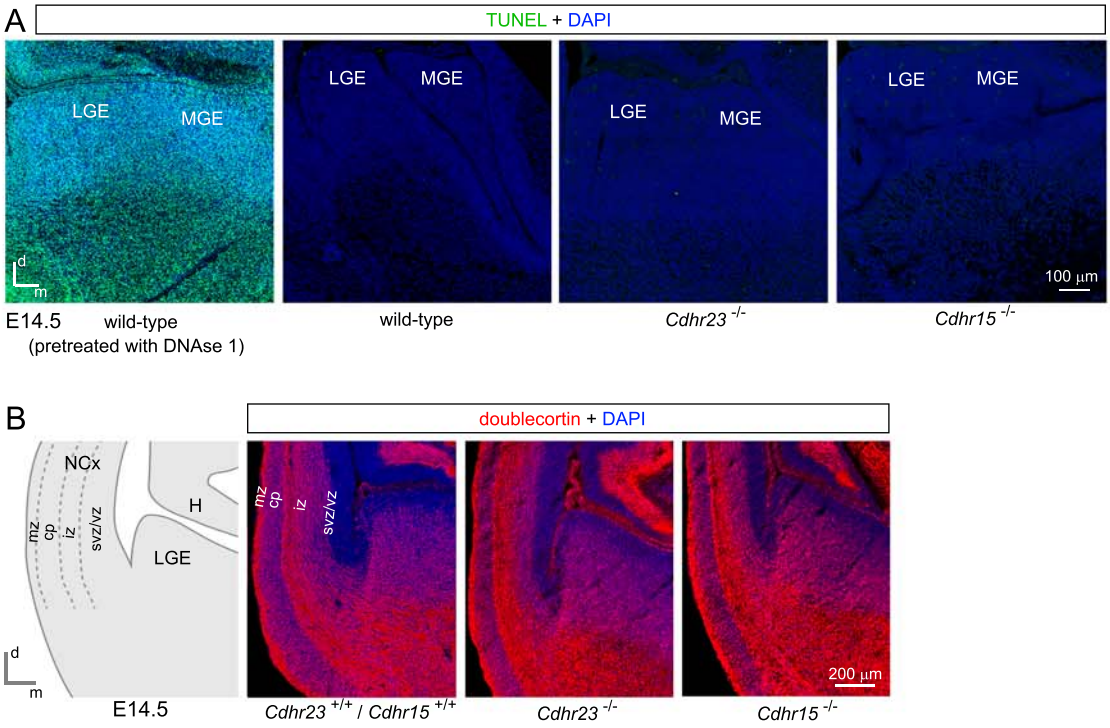

Supporting Information 6

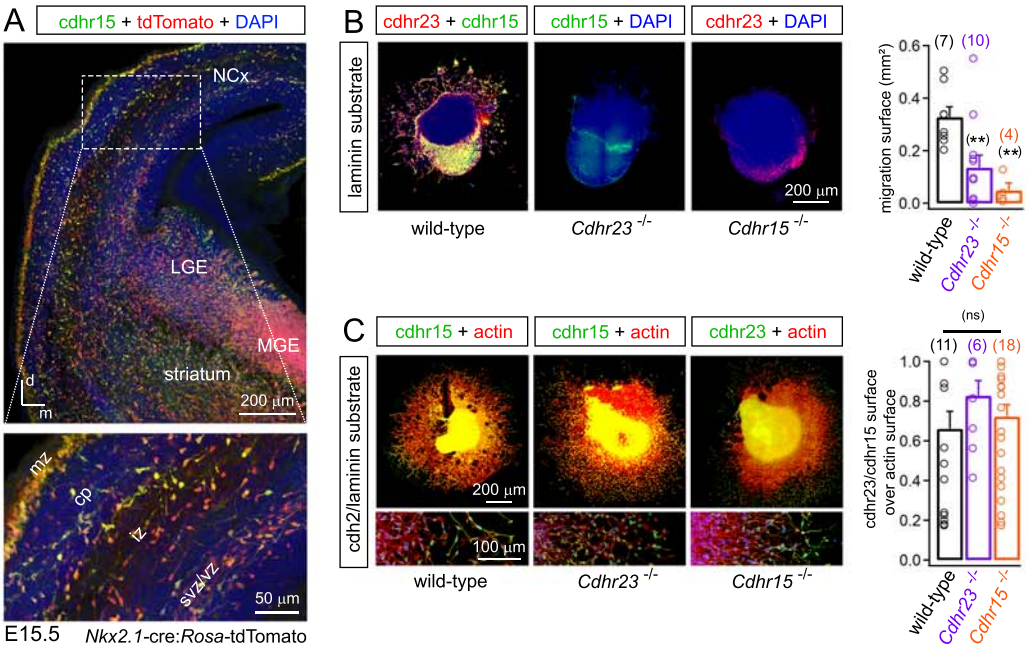

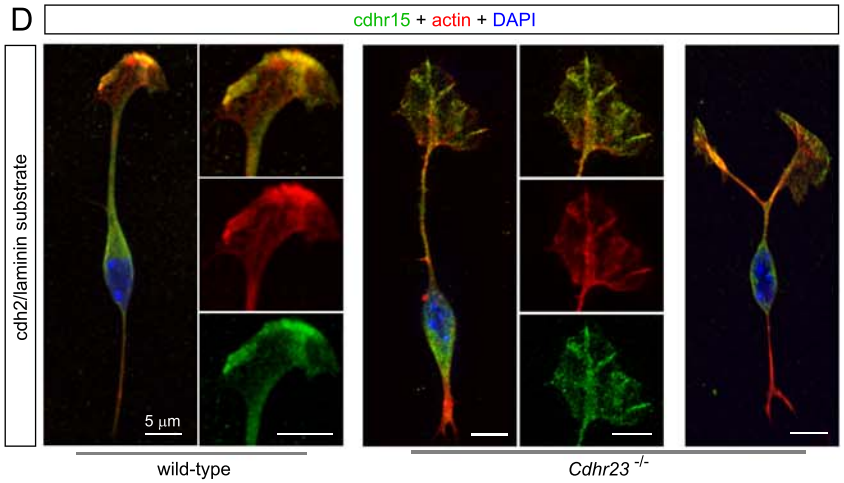

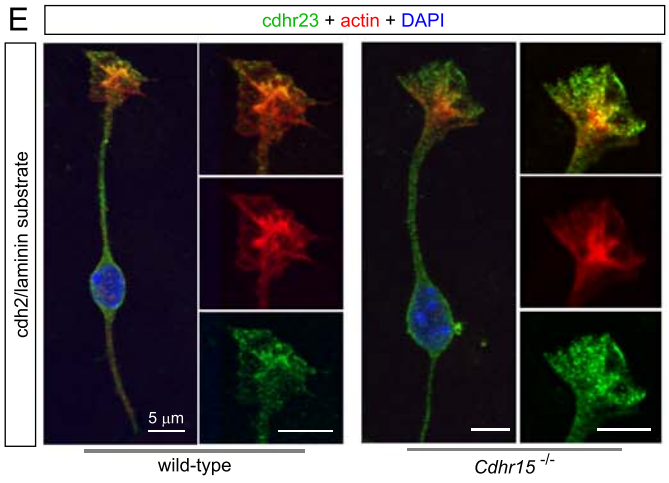

Supporting Information 7

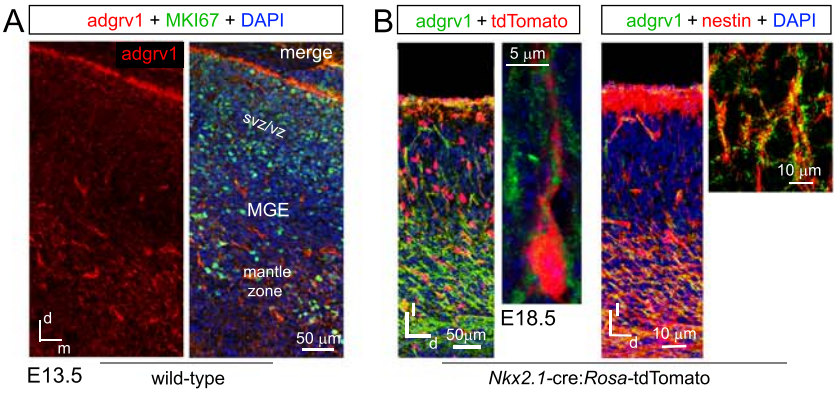

Supporting Information 8

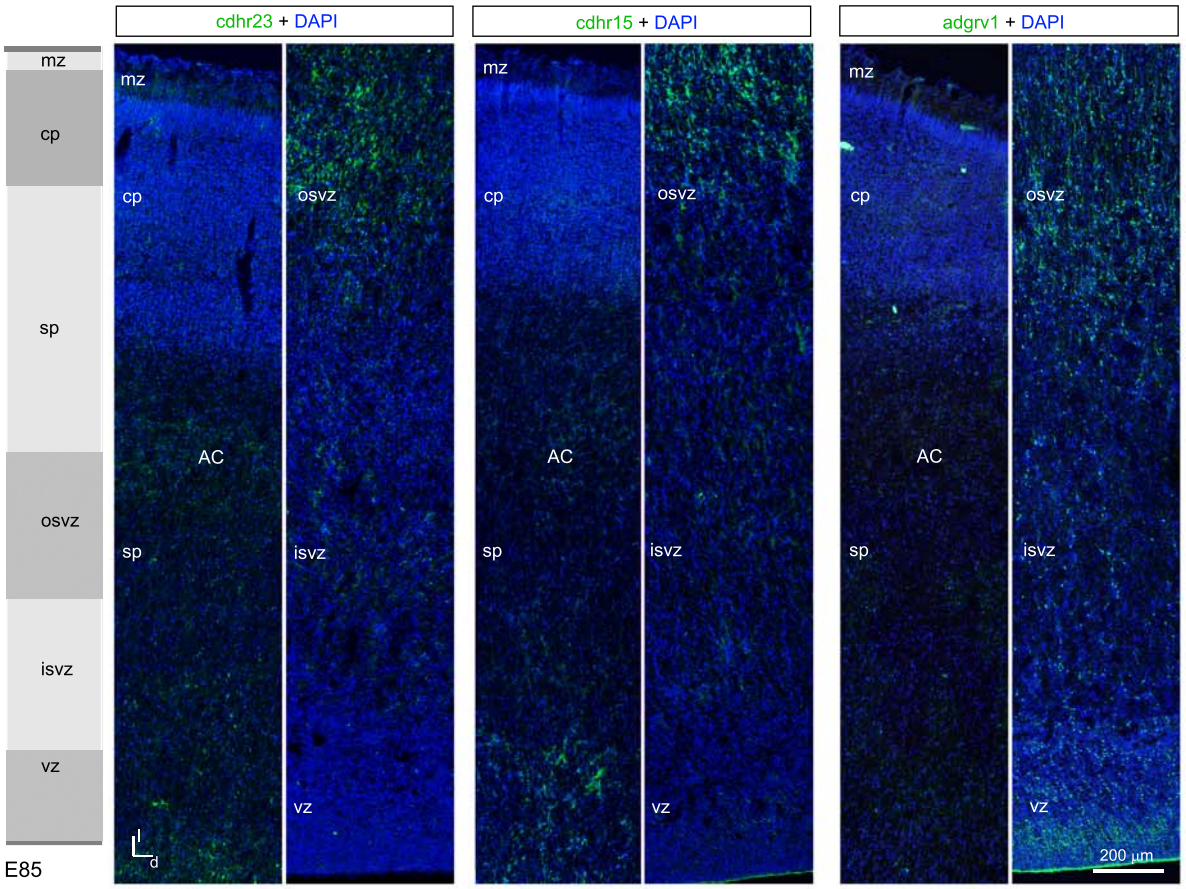

Supporting Information 9